THE ANTENNA LABORATORY

RESEARCH ACTIVITIES in ---

Automatic Controls | *Antennas* | *Echo Area Studies*
Microwave Circuits | *Astronautics* | *E M Field Theory*
Terrain Investigations | *Radomes* | *Systems Analysis*
Wave Propagation | | *Submillimeter Applications*

A PARAMETER STUDY OF A CARBON DIOXIDE GAS LASER

D. B. Rensch

Grant Number NsG-74-60

1093-34 15 November 1966

Prepared for:
National Aeronautics and Space Administration
Office of Grants and Research Contracts
Washington, D. C. 20546

Department of ELECTRICAL ENGINEERING

THE OHIO STATE UNIVERSITY
RESEARCH FOUNDATION
Columbus, Ohio

NOTICES

When Government drawings, specifications, or other data are used for any purpose other than in connection with a definitely related Government procurement operation, the United States Government thereby incurs no responsibility nor any obligation whatsoever, and the fact that the Government may have formulated, furnished, or in any way supplied the said drawings, specifications, or other data, is not to be regarded by implication or otherwise as in any manner licensing the holder or any other person or corporation, or conveying any rights or permission to manufacture, use, or sell any patented invention that may in any way be related thereto.

The Government has the right to reproduce, use, and distribute this report for governmental purposes in accordance with the contract under which the report was produced. To protect the proprietary interests of the contractor and to avoid jeopardy of its obligations to the Government, the report may not be released for non-governmental use such as might constitute general publication without the express prior consent of The Ohio State University Research Foundation.

REPORT 1093-34

REPORT

by

THE OHIO STATE UNIVERSITY RESEARCH FOUNDATION
COLUMBUS, OHIO 43212

Sponsor	National Aeronautics and Space Administration Office of Grants and Research Contracts Washington, D.C. 20546
Grant Number	NsG-74-60
Investigation of	Receiver Techniques and Detectors for Use at Millimeter and Submillimeter Wave Lengths
Subject of Report	A Parameter Study of a Carbon Dioxide Gas Laser
Submitted by	D. B. Rensch Antenna Laboratory Department of Electrical Engineering
Date	15 November 1966

The material contained in this report is also used as a thesis submitted to the Department of Electrical Engineering, The Ohio State University as partial fulfillment for the degree Master of Science.

ACKNOWLEDGMENTS

The writer wishes to express his appreciation to Dr. S. H. Koozekanani and Dr. H. Hsu for their constructive criticism and encouragement during the course of this work. The many helpful experimental techniques which were initiated by Mr. J. McCoy are deeply appreciated. Thanks are also due to Dr. P. K. L. Yin and Mr. E. K. Damon for their helpful comments.

The writer gratefully acknowledges that this work was performed in part while studying under a National Defense Education Act Fellowship in Quantum Electronics in the Department of Electrical Engineering, The Ohio State University.

ABSTRACT

The problem of defining some of the many parameters; such as, discharge tube width and length, gas flow rate, tube wall temperature, and gas mixtures, as they pertain to a CO_2 gas laser, is considered. The pertinent theory on symmetry properties of CO_2 and its ability to be used as an amplifying medium for infrared frequencies are presented, along with the techniques to be used in determining the effect the above-mentioned parameters have on laser action. The experimental results showed that the above parameters can be defined, therefore some of the guess-work in determining optimum laser action for a CO_2 gas laser can be removed. Also, laser operating frequency, symmetry properties, and amplifying characteristics of CO_2 can be correlated with theory.

CONTENTS

CHAPTER I
INTRODUCTION

A great deal of investigation has been done on CO_2 lasers since Patel first reported optical laser action on a number of rotational lines of the $\Sigma_u^+ - \Sigma_g^+$ vibrational band of CO_2.[1] Most of the work on lasers has been performed with fixed parameters (gas flow, discharge tube width and length, tube temperature, discharge current, and gas mixtures) but there is not a clear understanding of the role that these parameters play in the design of a CO_2 gas laser for optimum power.

The purpose of this report is to report the techniques used to vary the above parameters and to report the results observed in laser action as a function of these parameters. The laser used to facilitate this study was constructed with external windows and interchangable glass pipes. The CO_2 laser was cw-operated and was able to produce 25 watts of continuous power while operating on a number of rotational lines at about 10.6μ. Special attention was given to the study of the effect that helium gas has on laser action. A "double tube" arrangement was constructed for this study.

In the following section, there will be a brief review of symmetry properties of CO_2, with particular attention to properties which govern

laser action. The ability of the CO_2 laser to act as an amplifier of infrared frequencies is considered. The experimental procedure and results which are included indicate the optimum value of the parameters for maximum laser power.

CHAPTER II
THEORETICAL CONSIDERATIONS

A. Symmetrical Properties of Carbon Dioxide (CO_2)

1. Representations for the $D_{\infty}h$ symmetry group

CO_2 is a symmetric linear molecule belonging to the $D_{\infty}h$ symmetry group.[2,3] This group contains a horizontal reflection plane and two-fold symmetry about any axis in this plane passing through the molecular center. It also contains infinite fold symmetry about the molecular axis. Figure 1 shows these symmetry properties.

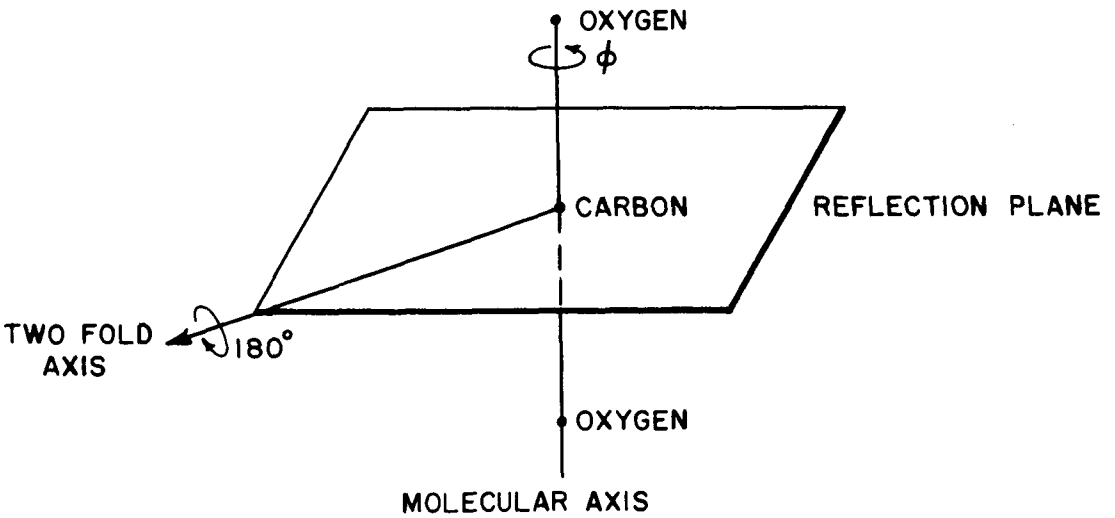

Fig. 1. Diagram illustrating symmetrical plane and axis for the CO_2 molecule.

To be able to determine certain properties of CO_2 using group theory; e.g., normal modes and allowable transitions, it is necessary to know the irreducible representation for the $D_{\infty h}$ group.[2,3,4] The following irreducible representation table and notation are taken from Tinkham.[3]

Table I. Representation table for the $D_{\infty h}$ symmetry group

$D_{\infty h}$			E	$2C_\phi$	C_2'	i	$2iC_\phi$	iC_2'
x^2+y^2, z^2		Σ_g^+	1	1	1	1	1	1
	z	Σ_u^+	1	1	1	-1	-1	-1
	R_z	Σ_g^-	1	1	-1	1	1	-1
		Σ_u^-	1	1	-1	-1	-1	1
(xz, yz)	(R_x, R_y)	π_g	2	$2\cos\phi$	0	2	$2\cos\phi$	0
	(x, y)	π_u	2	$2\cos\phi$	0	-2	$-2\cos\phi$	0
		...	.....					
		...	.....					

E is the unit operator of the symmetry group, C_ϕ is the rotation operator around the symmetry axis, C_2' is the 180° rotation about the two-fold axis, and $\underline{i}$ is the inversion operator. The other columns list the coordinates; quadratic forms of coordinates; and rotations R_x, R_y, R_z, about the coordinate axis to indicate the representation to which they transform.

2. Normal modes of CO_2

According to classical mechanics, 3N coordinates are needed to specify the positions of N nuclei. Three of these are X, Y, Z, and the three angles θ_i. The remaining coordinates are obtained by choosing any 3N-6 independent linear combinations of the displacements

$$\delta_\alpha = r_\alpha - r_{\alpha o} \tag{1}$$

and referring to these as the normal vibration mode coordinates. r_α is the displacement of the α^{th} nucleus from its equilibrium position $r_{\alpha o}$.

An arbitrary distortion or displacement of the molecule is made in order to determine the three normal modes of CO_2. This displacement may be specified by the nine vectors $\Delta_{x\alpha}$, $\Delta_{y\alpha}$, and $\Delta_{z\alpha}$ ($\alpha = 1, 2, 3$). The following diagram indicates these nine vectors.

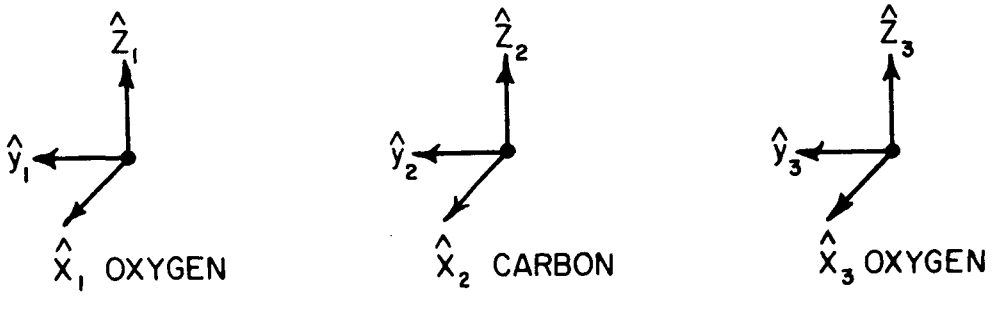

Fig. 2. Diagram illustrating displacement vectors for CO_2.

These vectors form the basis for a representation $\Gamma_{(total)}$ of the symmetry group $D_{\infty h}$ of the molecule. Applying the operators of

the group to these vectors yields the following:

$C_\phi \hat{y}_1 = \hat{y}_1$,

$C_2' \hat{y}_1 = -\hat{y}_3$,

$iC_\phi \hat{y}_1 = -\hat{y}_3$, and

$iC_2' \hat{y}_1 = \hat{y}_1$.

Similar operations with the remaining eight vectors gives the following representation table.

Table II. Nine-dimensional representation for CO_2.

	E	$2C_\phi$	C_2'	i	$2iC_\phi$	iC_2'
Γ_{total}	9	$3+6\cos\theta$	-1	-3	$-1-2\cos\theta$	3

From the $D_{\infty h}$ representation. $\Gamma_{(total)}$ may be reduced to the following modes:

$$\Gamma_{(total)} = \Sigma_g^+ + 2\Sigma_u^- + \pi_g + 2\pi_u . \tag{2}$$

Since $\Gamma_{(total)}$ is the total representation, the three translational modes and the three rotational modes must be subtracted from $\Gamma_{(total)}$ to give the vibrational modes. The translation modes account for the representation of x, y, z; namely, $\pi_u + \Sigma_u^-$. The three rotations remove π_g; this leaves:

$$\Gamma_{vib} = \Sigma_g^+ + \Sigma_u^- + \pi_u . \tag{3}$$

The following diagrams indicate the displacement of the CO_2 molecule for its three normal modes:

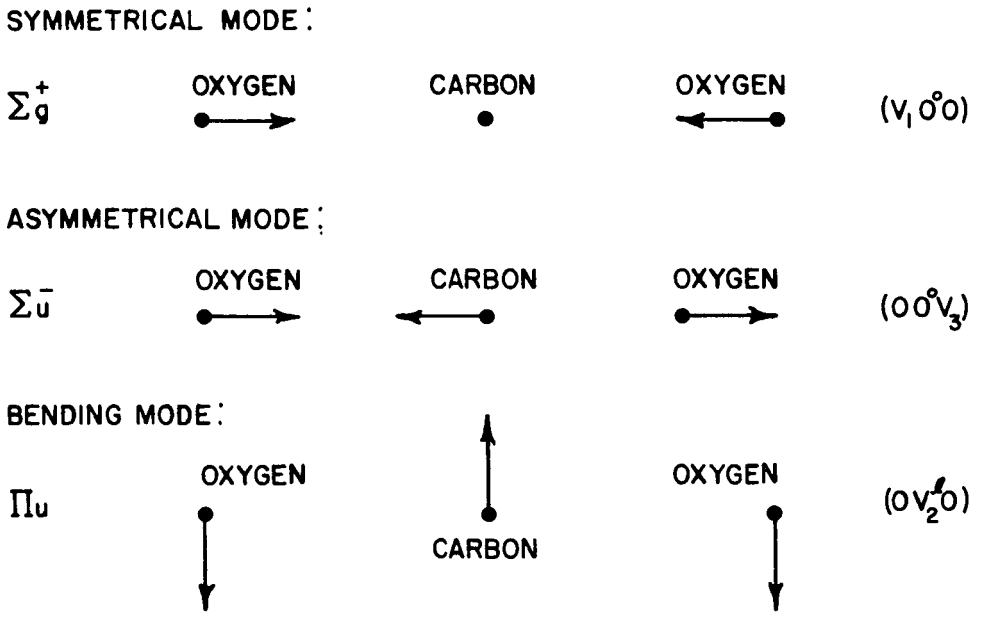

V_1, V_2, V_3 are the quanta of energy in that normal mode and ℓ is the angular momentum quantum number associated with the bending mode.[5] Therefore there are two non-degenerate modes, Σ_g^+ and Σ_u^-, and one degenerate mode, π_u.

The vibrational energy levels of CO_2 do not contain just these three normal modes, but the energy levels are a complex multilevel system formed by combinations, differences, and overtones of these modes. Figure 3 shows a partial vibrational energy level diagram for the CO_2 molecule.

3. Infrared spectra (vibrational)

Since the multilevel vibrational system has been discussed, the next step is to determine the selection rules corresponding to transitions between certain vibrational levels.

Because electric dipole transitions (those which are infrared active)[2, 3, 6] are important here the following rule may be used:[2]

> There is an infrared absorption line corresponding to the transistion V_{1b1} to V_{1b2} if, and only if, the representation $\Gamma_{(vector)}$ of one or more of the dipole moment components x, y, z is contained in the reduction of the representation $\Gamma_{(v1b\,1)} \times \Gamma_{(v1b\,2)}$.

For example, transitions between the vibrational states Σ_g^+ and Σ_u^+ are allowed since $\Sigma_g^+ \times \Sigma_u^+$ yields Σ_u^+ and the vector z transforms as Σ_u^+ (see Tabel I). In the above rule, the rotational degrees of freedom of the bending mode have been neglected and therefore the ℓ quantum number associated with the bending mode is not considered in the selection rules. The following selection rules are more general:[6]

(4) $|\nabla V_2|$ = even no.; $|\nabla \ell|$ = 0, $|\nabla V_3|$ = odd no.

(5) $|\nabla V_2|$ = odd no.; $|\nabla \ell|$ = 1 · $|\nabla V_3|$ = even no.

It should be noted that $|\nabla V_1|$ is not considered in the selection rules because of its symmetry. Figure 3 indicates some of the allowable

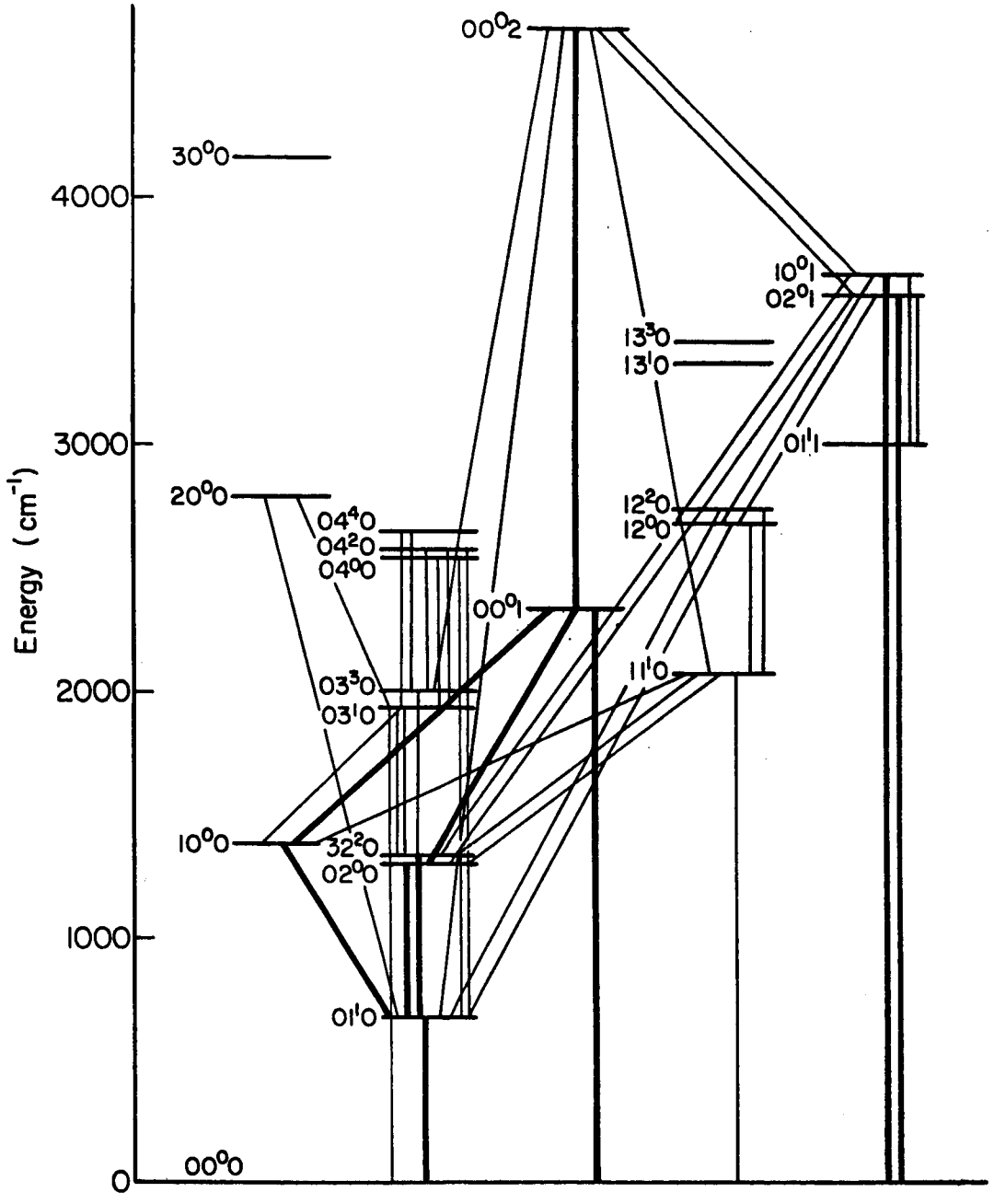

Fig. 3. A portion of the CO_2 infrared emission spectrum.

transitions by interconnecting lines; the dark lines indicate strong transitions.

4. Infrared spectra (rotational)

Considering now that the molecule has no vibration but only molecular rotation, it is possible to determine the infrared rotational spectra.

Transitions from one rotational energy level to another because of dipole radiation are permitted if the molecule has a permanent dipole moment. The permament dipole moment is invariant to operations of a group and therefore must transform according to the symmetrical representation Σ_g^+. The $D_{\infty h}$ group does not have a vector x, y, or z that transforms according to Σ_g^+; therefore, CO_2 has no permanent dipole and no rotational infrared spectra.

5. Vibrational-rotational interaction

To determine the energy of a vibrating and rotation molecule to the first approximation, the following expression is used:

$$E_{tot} = E_{vib} + E_{rot}.$$

Here it has been assumed that there is no coupling between vibrational modes and rotational modes, but the moments of inertia of the molecule are not independent of vibration and therefore coupling between the two modes occurs. Herzberg[7] has given the total energy of a vibrating-rotating linear molecule as

$$E_{(cm^{-1})} = \nu_o(V) + B(V)\,J(J+1) - D(V)\,J^2(J+1)^2 \qquad (6)$$

where $\nu_o(V)$ is the vibrational band center, B(V) is the corrected value of the "rotational constant" for the equilibrium position, D(V) is the corrected value of "centrifugal stretching constant," and J is the molecular rotational quantum number. For all practical purposes the third term may be neglected since $D(V) << B(V)$. The energy may be rewritten as

$$E(J) = \nu_o + B(V)\ J(J+1). \tag{7}$$

6. Rotational selection rules

The Wigner Echart theorem[8] yields the simple result that for transistions from one rotational level to another, the following selection rule must be observed:

$$\Delta J = \pm 1, 0, \tag{8}$$

where J is the rotational quantum number. Since the CO_2 molecule has two identical oxygen nuclei, rotation of the molecule by 180° effectively interchanges the two nuclei and therefore certain rotational lines are missing from the rotational spectra. Bose-Einstein and Fermi-Dirac statistics[5] require that the wave functions of identical particles must be symmetrical or antisymmetrical, respectively. Nuclear spin of oxygen I is equal to 0 and must behave as a boson particle (behave according to Bose-Einsteins statistics). To determine the missing lines, the procedure used by Tinkham[3] will be outlined here.

Tinkham interchanges the nuclei by the following series of operations:

1. Rotate molecule about an axis perpendicular to the molecular axis through an angle π,
2. invert electrons, and
3. reflect electrons though vertical plane.

It should be noted here that a rotation of π radians can be expressed as[8]

$$R(\pi) = e^{-i\pi J}.$$

Applying the above three steps to the Σ_u^+ representation yields

$$(-1)^J (-1) (+1) = (-1)^{J+1}.$$

The nuclear wavefunction must be symmetrical, therefore J must be an odd number for the Σ_u^+ representation. Next, the above operations are applied to the Σ_g^+ representation and the following result is obtained:

$$(-1)^J (+1) (+1) = (-1)^J.$$

For the wavefunction to be symmetrical, in this case, J must be even.

Thus, the above examples have shown that certain rotational energies are missing from a given vibrational level.

7. Summary

CO_2 is a vibrating-rotating symmetrical linear molecule consisting of a multilevel vibrational energy-level system superimposed with rotational energy levels. Transistions between these energy levels are governed by the following rules: (1) only certain rotational energy levels exist for a given vibrational level, and (2) certain selection rules must be followed for transitions between allowable energy levels.

B. CO_2 as an Amplifying Media

Previously, the writer has considered only symmetry properties of CO_2 and the use of CO_2 as an amplifying medium for a gas laser has not been discussed. An elementary treatment will now be considered.

Consider an electromagnetic wave incident upon an infinitesimal thickness (dx) of gas media.

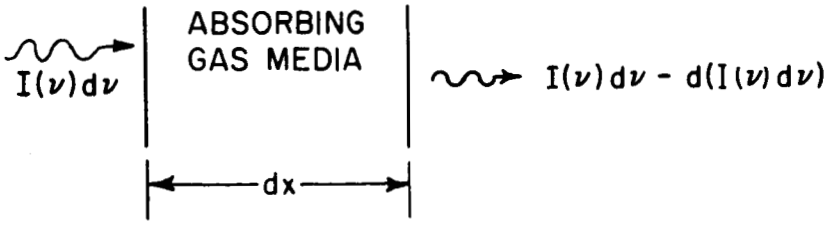

Fig. 4. Electromagnetic wave incident upon absorbing gas.

$I(\nu)$ is the intensity of the beam and

$$(9) \qquad d(I(\nu)\,d\nu) = dn_1 h\nu\, B_{12}\,\frac{I(\nu)}{4\pi}\,dx - dn_2 h\nu\, B_{21}\,\frac{I(\nu)}{4\pi}\,dx$$

is the change in the incident radiation because of the absorbing gas. dn_1 and dn_2 are the number of molecules per cc capable of absorbing the incident radiation between ν and $\nu + d\nu$ for the 1^{st} and 2^{nd} state, respectively; B_{12} and B_{21} are the Einstein B coefficients for induced absorption;[9] h is Planck's constant; and ν is the frequency. Assuming that the electromagnetic intensity $I(\nu)$ varies as a function of x

$$(10) \qquad I(\nu) = I_o e^{\alpha(\nu)x},$$

where $\alpha(\nu)$ is the gain coefficient per unit length and has a Gaussian distribution for low pressures.[9] Integrating both sides of Eq. (9) and substituting the proper values for $\alpha(\nu)$ and the B's, the following equation for $\alpha(\nu_o)$ (gain coefficient at center frequency ν_o) may be obtained:[10]

$$(11) \qquad \alpha_{J,J\pm1}(\nu_o) = \left(\frac{\ell n\, 2}{\pi}\right)^{\frac{1}{2}} \frac{16\,\pi^3 C^3}{3h\nabla V_D \lambda_o} \left|X_{J,J\pm1}\right|^2 \left(\frac{n_1 J}{g_J} - \frac{n_2\, J\pm1}{g_{J\pm1}}\right),$$

where ∇V_D is the full frequency width of the Doppler-broadened line at half-maximum gain, $\left|X_{J,J\pm1}\right|$ is the dipole matrix element between the rotational states J and $J \pm 1$ (follows selection rules given by Eq. (8)),[11] and g_J and $g_{J\pm1}$ are statistical weights equal to

the degeneracy of the energy level. If for a given vibrational level the rotational level population n_J is given by a Boltzman distribution for a given temperature T, then Herzberg[6] shows that

$$(12) \qquad n_J = n\, g_J\, hC\, B(V)\, e^{-B(V)\, J(J+1)\, \frac{hC}{kT}},$$

where K is Boltzman's constant. Combining Eq. (12) and (11), replacing ∇V_D with its proper value, and replacing $|X_{J,\,J+1}|^2$ with A(J+1) where A is a constant independent of J, the final expression for $\alpha(\nu_o)$ may be written

$$(13) \quad \alpha_{J,\,J+1}(\nu_o) = \frac{8\pi^3 C^4 A}{3KT} \left(\frac{2\pi KT}{M}\right)^{-\frac{1}{2}} (J+1) \left[n_1 B(V_1)\, e^{-B(V_1)\, J(J+1) \frac{hC}{kT}} - n_2 B(V_2)\, e^{-B(V_2)\, (J+1)(2J+1) \frac{hC}{kT}} \right]$$

and

$$(14) \quad \alpha_{J,\,J-1}(\nu_o) = \frac{8\pi^3 C^4 A}{3KT} \left(\frac{2\pi KT}{M}\right)^{-\frac{1}{2}} \cdot (J) \left[n_1 B(V_1)\, e^{-B(V_1)\, J(J+1) \frac{hC}{kT}} - n_2 B(V_2)\, e^{-B(V_2)\, (2J)\, (J-1)\, \frac{hC}{kT}} \right],$$

where M is the molecular mass. Patel[10] has plotted in Fig. 5 Eqs. (13) and (14) for the following conditions:

(1) 1st level (lower level) is the 00°1 state of CO_2,

(2) 2nd level (upper level) is the 10°0 state of CO_2,

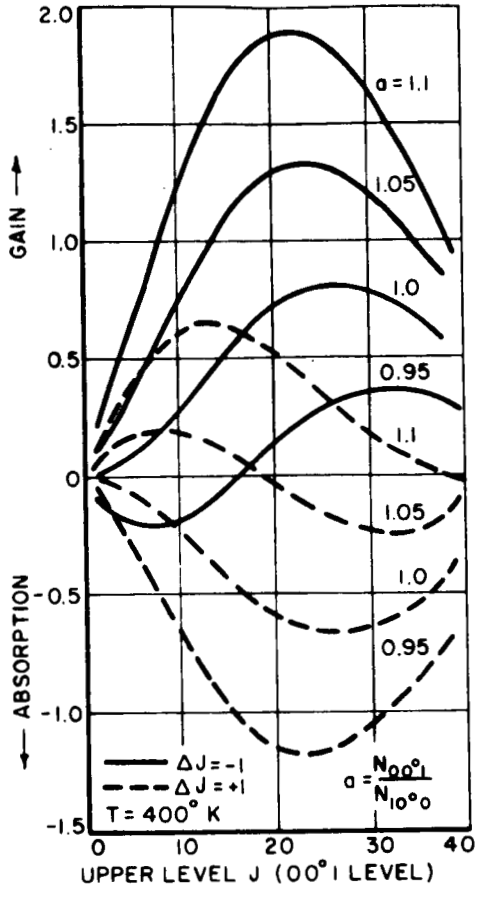

Fig. 5. CO_2 amplifier gain per pass as a function rotational quantum number J and vibrational ratio level $a = \frac{N_{00^\circ 1}}{N_{10^\circ 1}}$.

(3) discharge temperature T = 400°K, and

(4) normalized to $\frac{8\pi^3 C^4 A N_2}{3KT\left(\frac{2\pi KT}{M}\right)^{\frac{1}{2}}}$.

Thus, assuming that the necessary conditions for feedback are satisfied, the only further requirement necessary for oscillation is that the gain per pass supplied by the CO_2 gas medium be at least as great as the magnitude of the total losses per pass. Then

from Fig. 5 it is seen that for a given loss a certain population inversion will satisfy the conditions for oscillations.

C. Theory of CO_2 Lasers

Laser action in CO_2 gas has been reported on a number of wavelengths in the 10μ region.[10,12,13] The following analysis and experimental work will deal primarily with the $\Sigma_u^+(00°1)$ to $\Sigma_g^+(10°0)$ vibrational transition near 10.6μ. Figure 6 illustrates the energy levels for both pure CO_2 and N_2-CO_2 lasers. For simplicity the rotational levels are not shown.

Application of the selection rules discussed in section A(3) to the upper laser level, CO_2 $\Sigma_u^+(00°1)$, and the ground level, CO_2 $\Sigma_g^+(00°0)$, in pure CO_2 shows that the transition is allowed. The upper laser level which is located 2349.3 cm^{-1} above the ground state is populated by electron impact from the ground state, $\Sigma_g^+(00°0)$, as well as by recombination and cascades from higher energy levels.[1] In the N_2-CO_2 gas laser, the CO_2 $\Sigma_u^+(00°1)$ level has an additional population mechanism; i.e., population by transfer of vibrational energy from nitrogen molecules in the $N_2(V=1)$ vibrational level. Figure 6 shows the energy level $N_2(V=1)$ located 2330.7 cm^{-1} above the ground level. It is evident that the $N_2(V=1)$ level is nearly coincident with the CO_2 $\Sigma_u^+(00°1)$ vibrational level, the difference in energy being approximately 18 cm^{-1}. Thus the

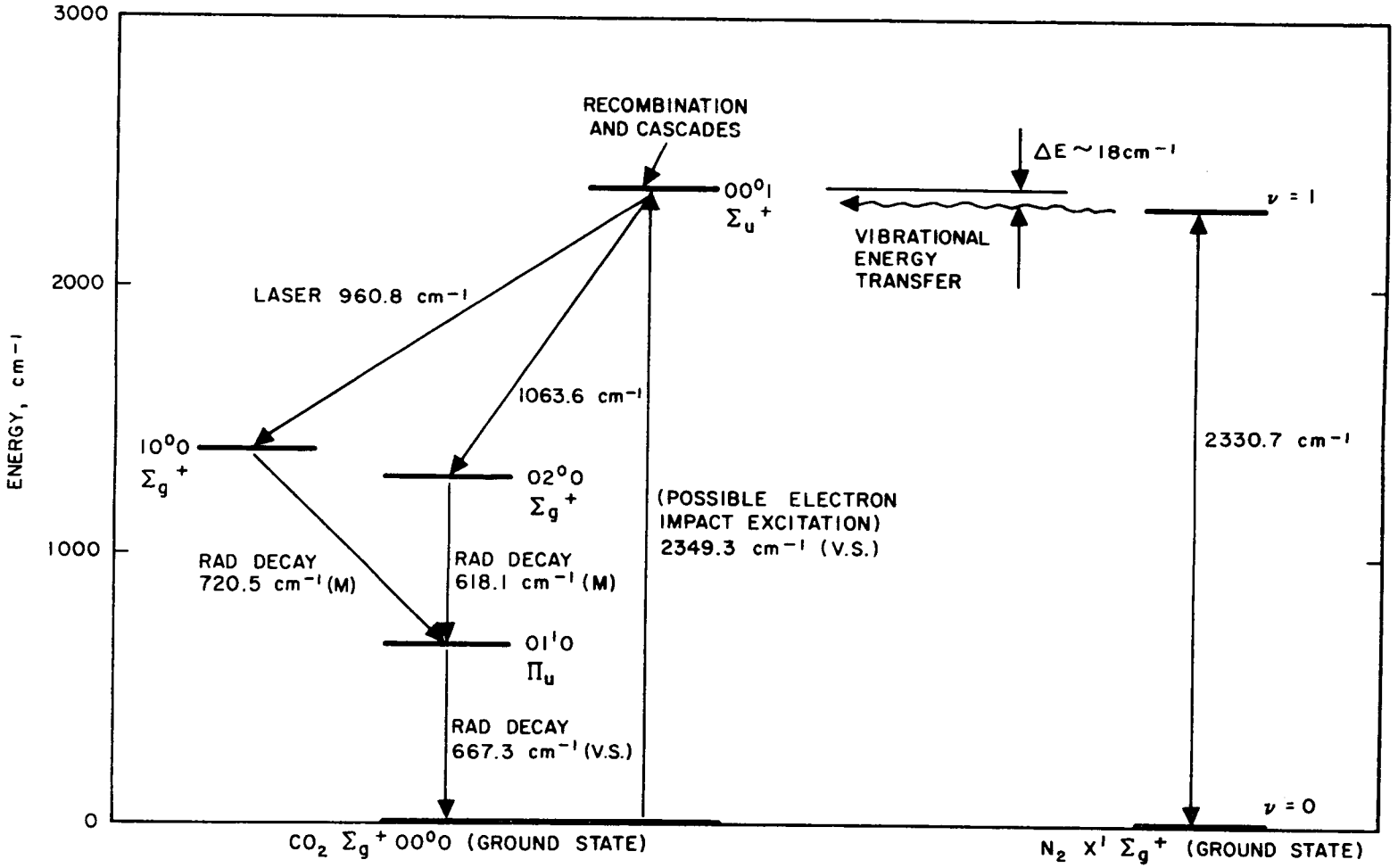

Fig. 6. Energy level diagram showing pertinent levels in CO_2 and N_2.

collision transfer of vibrational energy of this kind may be written as

(15) $$N_2(V=1) + CO_2(00^\circ 0) \rightarrow N_2(V=0) + CO_2(00^\circ 1) - 18\ cm^{-1}.$$

The validity of Eq. (15) is dependent on several factors. First, N_2 has a zero permanent dipole moment and therefore molecules excited to the V = 1 vibrational level cannot decay to the V = 0 ground level through electric dipole transitions. Thus the lifetime of the v = 1 vibrational level is governed by collisions with other molecules and the wall of the discharge tube. Bates[14] has shown that for collisions of the second kind and with reactions of the same energy difference as that in Eq. (15), the collision cross section is smaller than that for the case of excitation of CO_2 to the upper laser level described in Eq. (15), in which one of the transitions is forbidden. Secondly, Schwartz, Slawsky, and Herzfeld[15] have shown that the probability of transfer of energy between two different energy levels increases as $\triangle E$ decreases. Thus it is evident that $N_2(V=1)$ selectively populates the CO_2 $\Sigma_u^+(00^\circ 1)$ level.

The dominant relaxation of $\Sigma_g^+(C_2(10^\circ 0)$ is, according to Weber and Deutsch,[16] by vibration-vibration exchange with the binding mode Σ_g^+ CO_2 $(02^\circ 0)$. This is true because the near resonance of the $\Sigma_g^+(10^\circ 0)$ level with the Σ_g^+ $(02^\circ 0)$ level allows rapid transfer of vibrational energy by collisions. The vibrational energy transfer

may be written as

(16) $CO_2(10°0) + CO_2(00°0) \rightarrow CO_2(00°0) + CO_2(02°0)$.

The transition of the $\Sigma_g^+(02°0)$ vibrational level to the $\pi_u(01'0)$ level is by vibrational-translational relaxation. For the relaxation of the $\pi_u(01'0)$ level, it has been shown that vibrational-translational relaxation of CO_2 is most probable for vibrational quanta of the lowest frequency V_2 in which

(17) $CO_2(01'0) + M \rightarrow CO_2(00°0) + M +$ Kinetic energy,

where M is a CO_2 molecule. In all cases given above, the final relaxation is governed by Eq. (17).

CHAPTER III
THE CO_2 LASER EXPERIMENT

A. Experimental Set-up

For the proposed research of the CO_2 gas molecular laser to be investigated, the writer found that Kimax Tempered Glass pipe allowed the necessary discharge tube configurations to be easily constructed. The glass pipe was obtained in various lengths, widths, and configurations. Figure 7 shows some of the different glass pipe used to construct the laser for this experiment. With this flexibility, the discharge tube length could be varied from 38 to 160 cm with a fixed tube width of 1.90 cm. The width varied from 0.95 to 3.80 cm with a fixed tube length of 115 cm.

Gas pressure in the discharge tube was measured with an Alphatron Vacuum Gauge. All experiments conducted with this laser were with a flowing gas system and the vacuum gauge was connected so that pressure at either end of the discharge tube could be separately measured (see Figs. 8 and 9).

On the ends of the discharge tube were mounted specially designed infrared window holders. Essentially the holders consisted of a block of aluminum with a 2.50 cm diameter hole through the center and aligned with the discharge tube. One end of the aluminum block was faced off so that it would fit tightly against an o-ring in the glass pipe, while the other end of the block had a flat surface cut at the

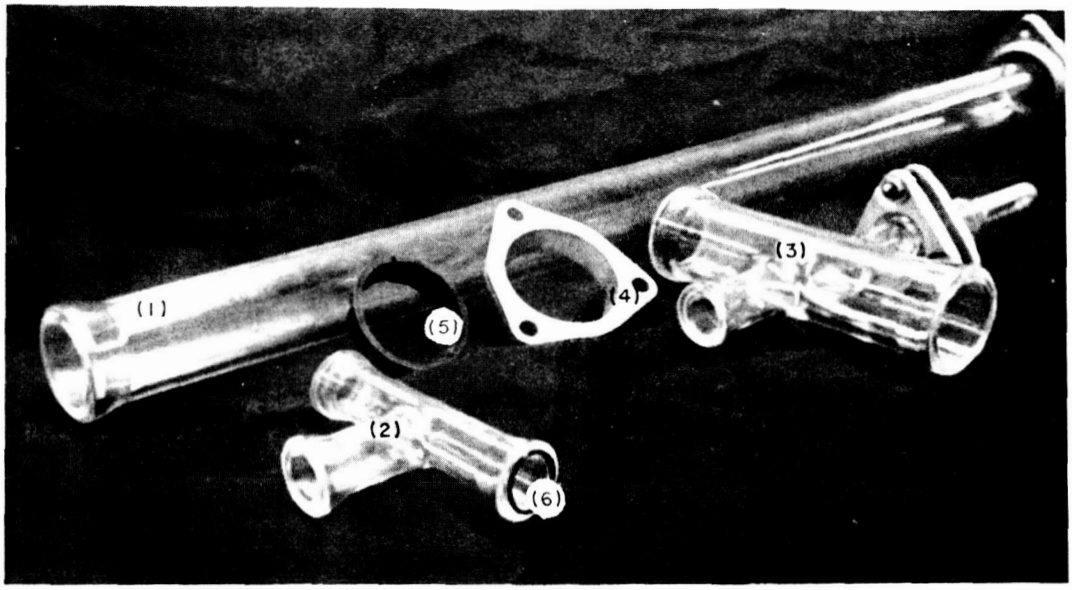

Fig. 7. Photograph of glass pipe used in experimental setup: (1) 76 cm straight glass pipe, (2) 1.9 cm glass tee, (3) 38 cm glass cross, (4) aluminum flange, (5) gasket, (6) o-ring.

Brewster angle for sodium chloride (salt). This surface contained an o-ring on which a 60 by 7 mm circular salt flat lay (see Fig. 9).

The discharge tube was located between two spherical mirrors with radii of 4.0 meters and spaced approximately 2.5 meters apart. Thus for this nonconfocal resonator, the radius of the spot size for the fundamental mode may be determined from Boyd and Gordon.[17] In general, the spot size for the fundamental mode at a distance d/2 from the center of the resonator is given by

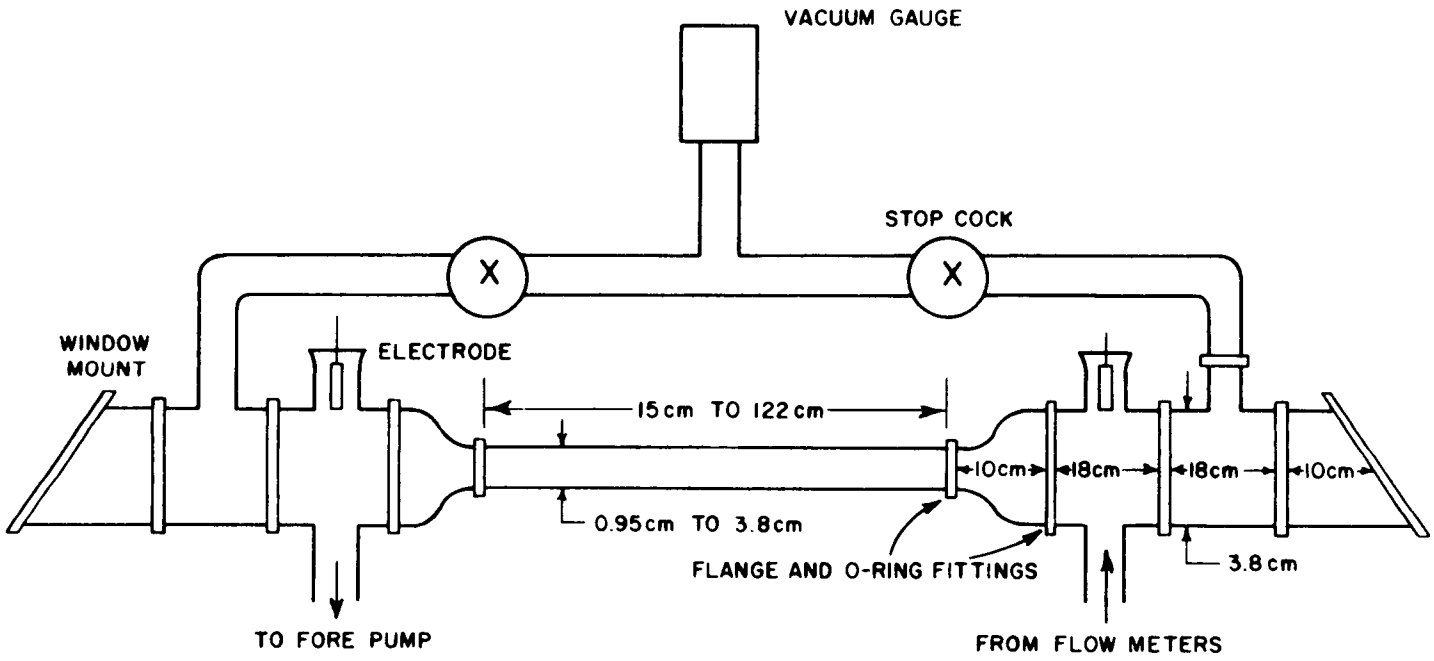

Fig. 8. The laser tube arrangement.

$$\omega_s' = \left(\frac{d\lambda}{\pi}\right)^{\frac{1}{2}} \left[\frac{2d}{b} - \left(\frac{d}{b}\right)^2\right]^{-\frac{1}{4}},$$

where d is the mirror separation, b is the mirror radius, λ is the oscillator wavelength. Using 10.6×10^{-6} meters for λ and the above-mentioned values for b and d, the radius is computed to be 5.2 mm.

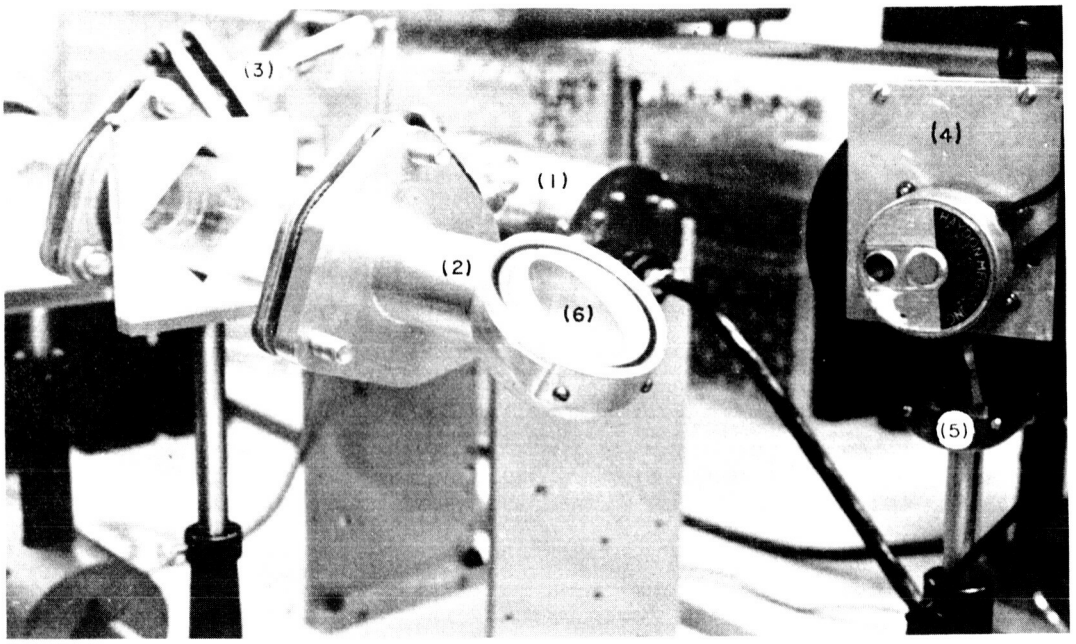

Fig. 9. Photograph of experimental setup: (1) vacuum gauge, (2) I. R. window holder, (3) electrode, (4) chopper, (5) I. R. detector, (6) sodium chloride windows.

Both mirrors which formed the resonator cavity were gold coated. The output mirror contained a 2.0 mm hole for coupling out the energy from the resonator cavity. Both mirrors were

mounted on a two-gimbal suspension mount; each had a 1.0-second resolution.

Gas flow through the discharge tube was measured with Fischer and Porter flowmeters. They consisted essentially of a tapered, calibrated glass tube with a spherical float inside. As flow rate increases the float rises. By reading the scale directly across from the float, flow rate is determined (see Fig. 10).

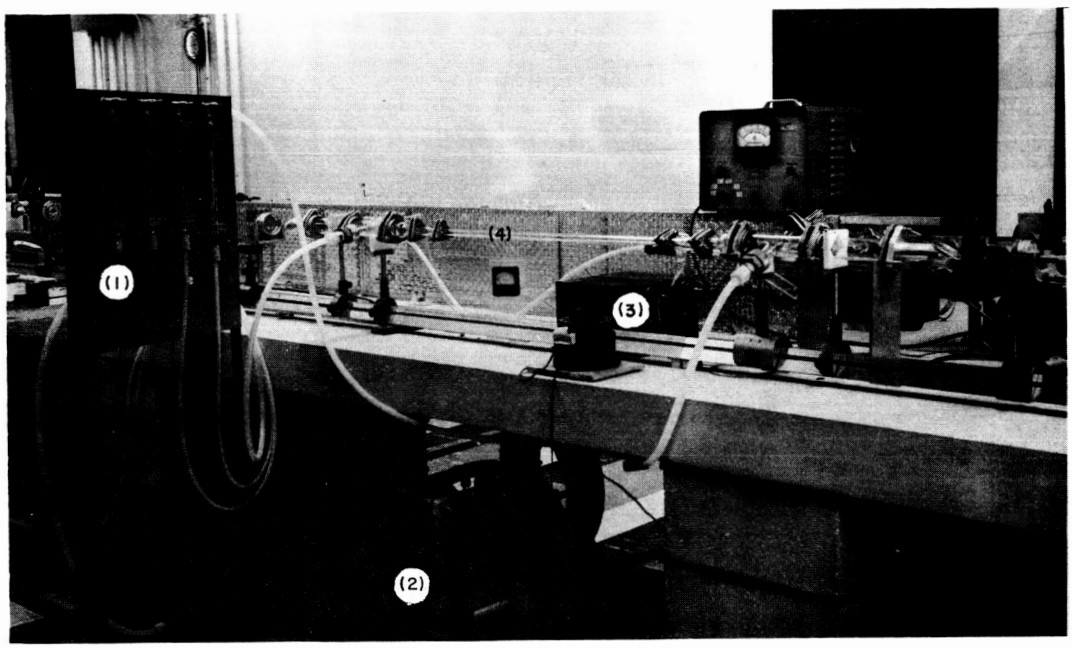

Fig. 10. Photograph showing experimental setup:
(1) flow meters, (2) fore pumps,
(3) transformers, (4) discharge tube.

Gas in the discharge tube was excited by two General Electric luminous tube transformers, each having the following ratings: secondary voltage 12,000 Vac, secondary current 60 mA. For

electrodes, Tubelite, A15 no-sputter electrodes were found to give good results.

Laser power was measured with a calibrated Eppley Thermopile detector. The laser power output exceeded the ratings of the detector and therefore it was necessary to reduce the input power to the detector. A chopper wheel rotating at 450 rpm was placed in front of the detector to reduce the input approximately 1.5 per cent. It should be noted here that since the output of the laser is quasi pulsed by the 60 cycle power supply, the phase of the chopper wheel with respect to the laser pulses will affect the amount of power entering the detector.

Laser wavelength was measured with a Perkin-Elmer, 112G, double-pass monochromator using a 75 ℓ/mm grating (see Fig. 11). The output of the monochromator feeds into a Leeds and Northrup chart recorder. Calibration was made with the 20th order of 0.5461μ mercury green line. The writer estimated that the accuracy of the measurements was better than 0.1 cm^{-1}. Figure 12 is a diagram of the basic experimental setup.

To determine the effect of tube wall temperature on laser power, a cooling jacket was placed around the 1.9-cm diameter glass pipe and pre-cooled methyl alcohol was forced through them. The methyl alcohol was cooled by passing it through a cooling coil that was surrounded by a solution of dry-ice and methyl alcohol.

Flow was produced by an electric fuel pump and flow rate was controlled by opening and closing a valve in the line. Wall temperature from -35°C to 40°C were obtained by adjusting the control valve. Figure 12 shows the experimental setup.

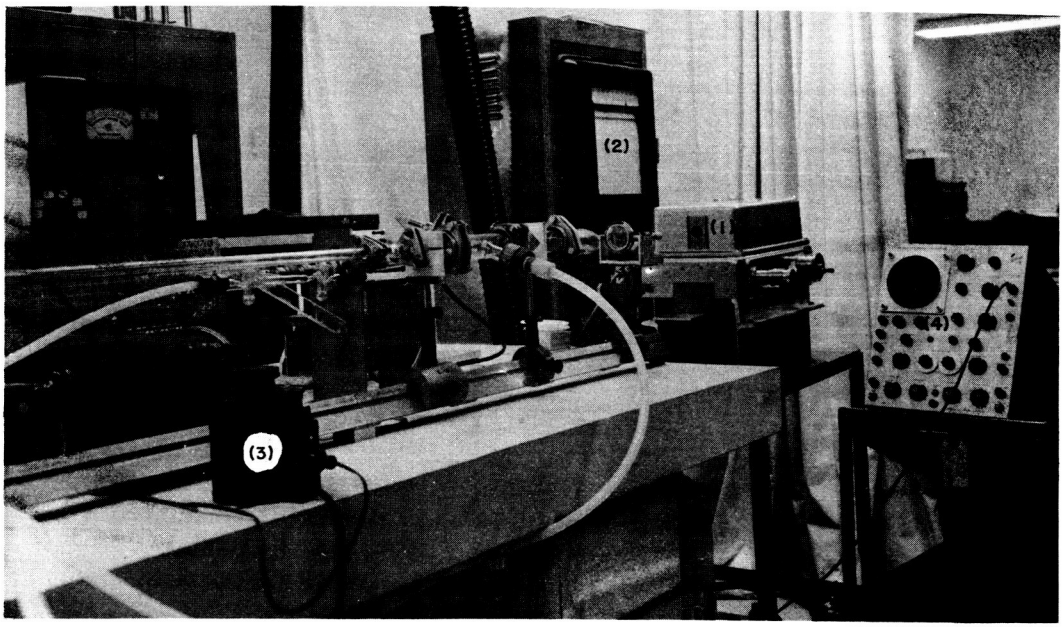

Fig. 11. Photograph of experimental setup: (1) monochromator, (2) chart recorder, (3) 0-115 VAC variac, (4) oscilloscope.

B. Experimental Results

1. CO_2 Gain and Laser Wavelength

Tables III and IV give the wavelengths at which laser oscillation was obtained. Table III lists the wavelengths which belong to the $\Delta J = -1$ or P-branch rotational transition of the $\Sigma_u^+(00°1) - \Sigma_g^+(10°0)$ vibrational band of CO_2. Table IV gives a similar description for the $\Sigma_u^+(00°1) - \Sigma_g^+(02°0)$ vibrational band.

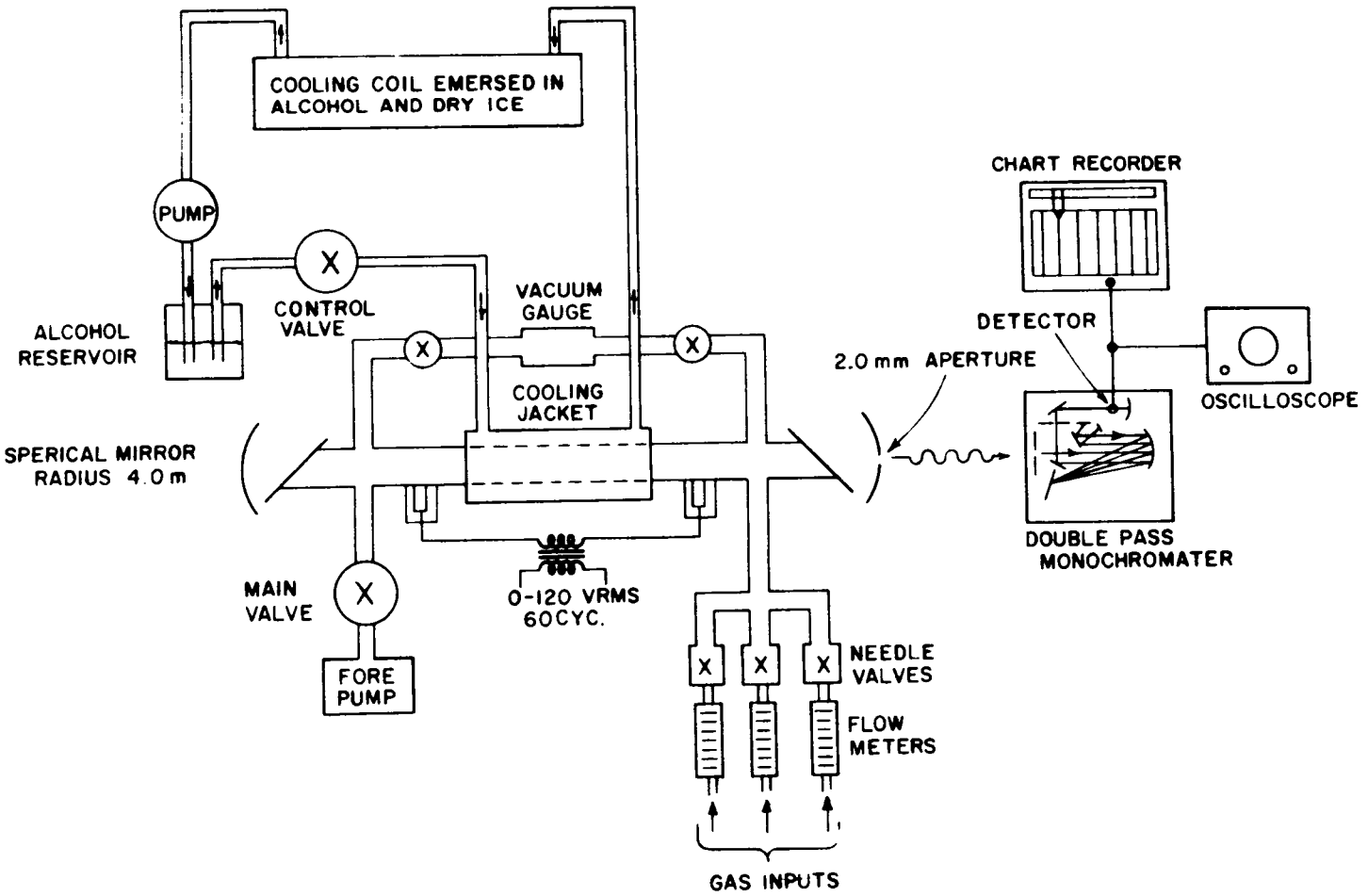

Fig. 12. Diagram of experimental setup used for measurements.

Table III. cw laser oscillation wavelength in the 00°1-10°0 band of CO_2

Measured Wavelength (μ)	Frequency (cm^{-1})	Transition 00°1-10°0 Band
10.533	949.39	P(14)
10.551	947.77	P(16)
10.570	946.07	P(18)
10.590	944.28	P(20)
10.610	942.50	P(22)
10.631	940.64	P(24)
10.652	938.79	P(26)

Table IV. cw laser oscillation wavelength in the 00°1-02°0 band of CO_2

Measured Wavelength (μ)	Frequency (cm^{-1})	Transition 00°1-02°0 Band
9.536	1048.6	P(18)
9.553	1046.7	P(20)
9.569	1045.0	P(22)
9.586	1043.2	P(24)
9.606	1041.0	P(26)
9.621	1039.4	P(28)
9.639	1037.4	P(30)

It is possible to determine the band center frequencies for Eq. (7) by using the above tables and the B(V) values taken from Reference 18; $B(00°1) = 0.38712\ cm^{-1}$, $B(10°0) = 0.38895\ cm^{-1}$, and $B(02°0) = 0.39173\ cm^{-1}$. Table V lists the results.

Table V. Band center frequencies for the 00°1-10°0 and 00°1-02°0 vibrational bands of CO_2

Band	Measured Center (cm^{-1})	Measured Ref. (19)
00°1-10°0	960.69	960.77
00°1-02°0	1064.1	1063.57

Measuring the wavelengths in the 9.6μ region was the extent of experimental work performed for this transition. The remaining results to be discussed will be for the 10.6μ transition. It should be mentioned here that it was necessary to use Kodak Irtran 2 infrared windows to permit oscillation in the 9.6μ region rather than sodium chloride windows which were used for the 10.6μ region. Irtran 2 windows were not used for the 10.6μ region because of its decreasing transmittance at wavelengths greater than 10.0 μ. Also, the Brewster angle for the window holders is designed for salt and therefore if Irtran 2 windows were used, additional loss would be added to the cavity because of partial reflection of the incident field.

As was discussed in Section IIB, the gain or absorption per pass of CO_2 is a function of population inversion. Thus, it is possible to determine this variable by determining the gain per pass as a function of rotational J numbers. Figure 13 illustrates the experimental setup used.

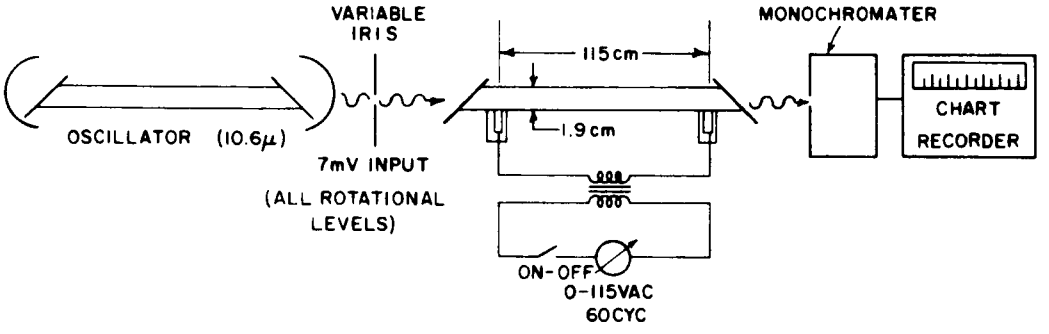

Fig. 13. Illustration of experimental setup for measurement of CO_2 amplifier gain per pass as a function of rotational quantum numbers J.

A CO_2 laser operating at the 10.6μ region was used for an oscillator. The energy from the oscillator was coupled out of its cavity through a 2.0 mm aperture and passed through a variable iris. The iris was adjusted to maintain a constant input for each rotational level into the 10.6μ amplifier. The 10.6μ radiation then passed through the CO_2-N_2-He amplifier (the addition of helium will be discussed later) and into the monochromator. The gain per pass is the difference in the radiation power received when the amplifier is on from that received when the amplifier is off.

It should be noted that all seven rotational lines from the oscillator are passing through the amplifiers, but only one is accepted by the monochromator. The writer felt that if the input signal were small (in the case the input power was approximately 7 mW, the error in the gain measurements would be negligible. The results of the measurement are plotted in Fig. 14. With the aid of Fig. 5 and an assumed discharge temperature of 400°K, the population ratio n 00°1/n 10°0 is found to be approximately 1.2. Patel[10] found a population ratio of 1.05 for pure CO_2. Thus, the addition of N_2 and He gases increased the population inversion.

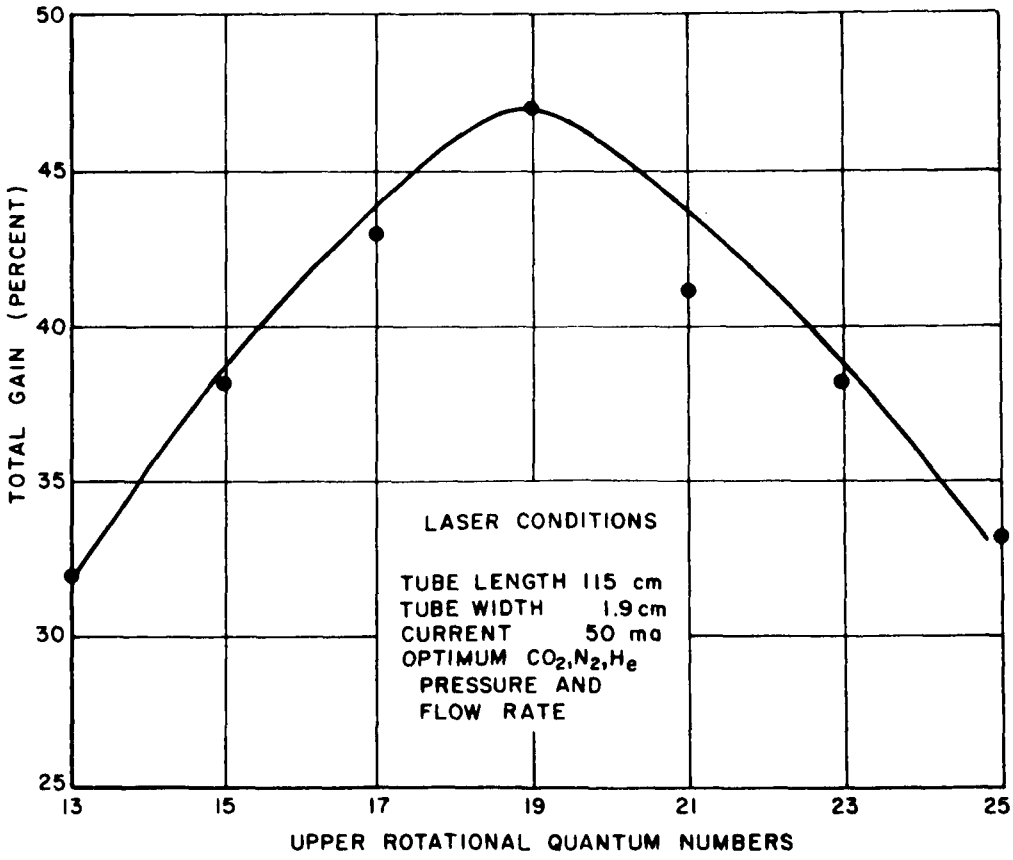

Fig. 14. Small signal gain per pass for CO_2 00°1-10°0 transition.

2. Effect of helium gas on CO_2-N_2 laser action

The effect of increased power from a gas laser with the addition of helium gas has been and still is under investigation by many workers.[16, 20, 21] In Fig. 15 the laser power found for CO_2-N_2, CO_2-He, and CO_2-N_2-He has been plotted as a function of discharge currents. For CO_2-N_2, maximum power is obtained at currents which barely sustain gas ionization and power is decreased steadily with larger currents. For the gas mixtures which contain He, the current corresponding to peak laser power approximately doubles, and for the CO_2-N_2-He mixture, the maximum laser power is six times that of CO_2-N2. Also, it should be noted that the CO_2-He mixture produced more laser power than the CO_2-N_2 mixture.

For a further study of the effect of He on CO_2 lasers, a "double-tube" arrangement was constructed. Figure 16 illustrates this arrangement. $N_2(V=0)$ enters through entrances 1 and 4 and passes through the discharge region where electron excitation produces $N_2(V=1)$. $CO_2(00°0)$ enters through entrances 2 and 3 and passes through the mixing region along with $N_2(V=1)$. Because of the selective excitation ability of $N_2(V=1)$, which was discussed in Section IIC, $CO_2(00°1)$ vibrational levels are produced. Since there is no discharge in the mixing region, population of the $CO_2(00°1)$ level must be strictly a result of exchange of energy with $N_2(V=1)$.

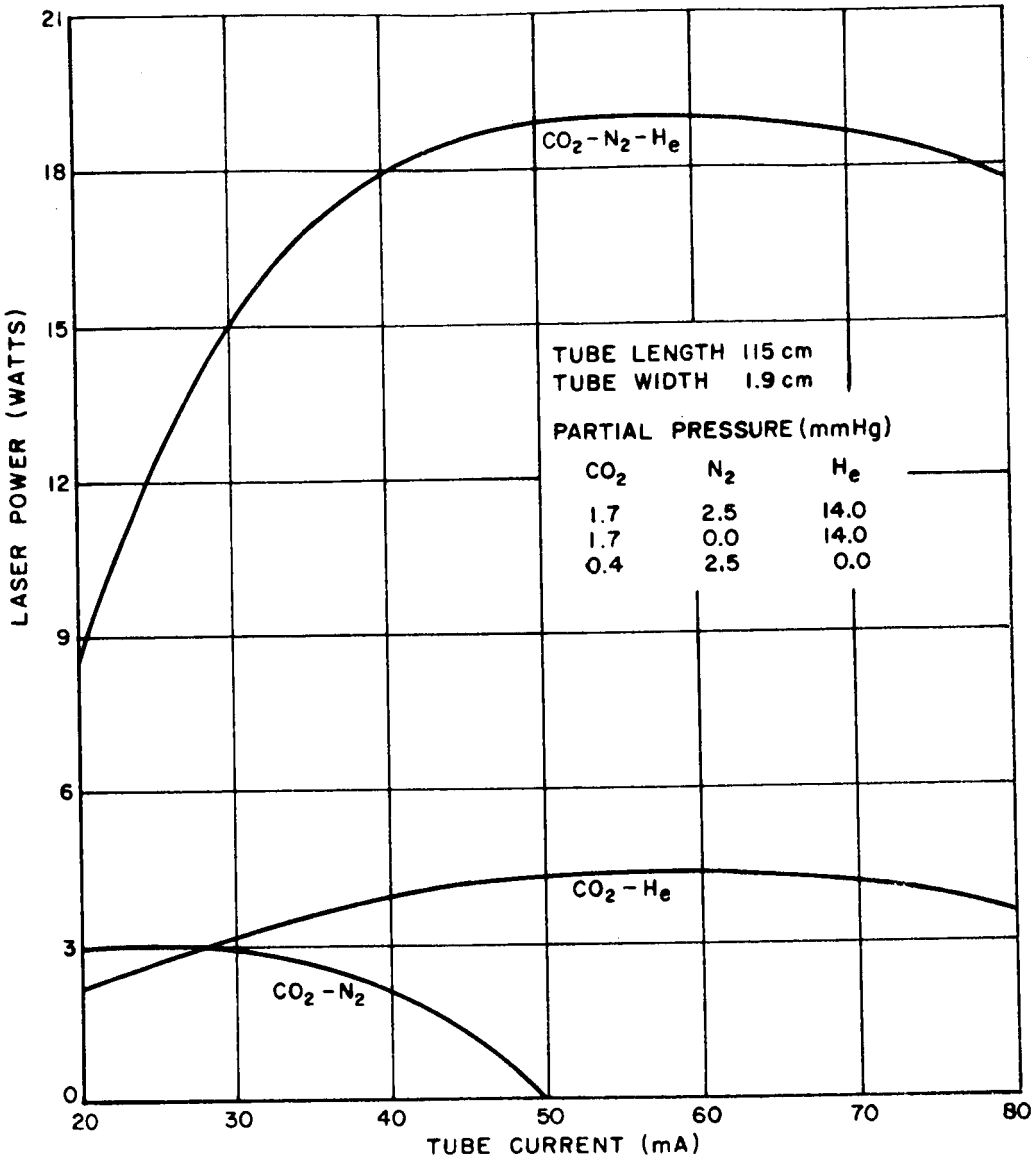

Fig. 15. CO_2 laser power curves for optimum mixtures of flowing gases.

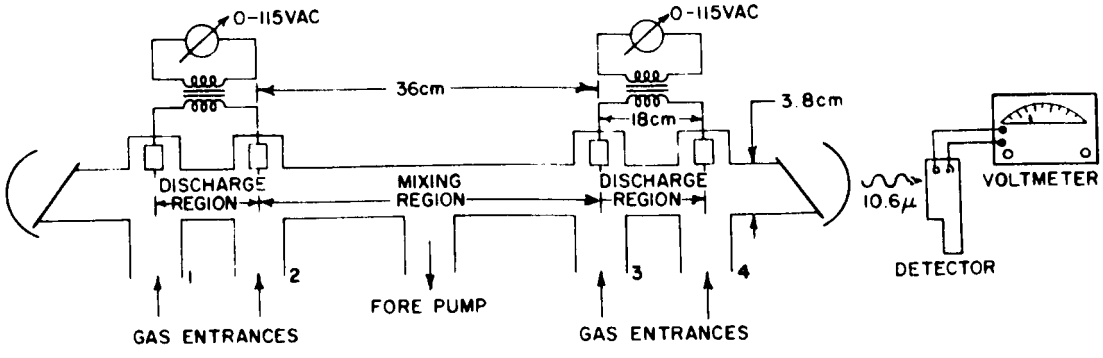

Fig. 16. "Double-tube" CO_2-N_2-He laser.

Laser action was obtained with the following gas pressures: CO_2 = 1.4 mm, N_2 = 850μm. Output was so weak that detection was possible only with the monochromator. Helium gas was then added at entrances 2 and 3 in order to study the effect of unexcited He on laser action. A plot of the results in Fig. 17 indicates an increase in the power output by a factor greater than the factor 6 which was given for the CO_2-N_2-He laser. Helium was then removed from entrances 2 and 3 and added at entrances 1 and 4. Laser action

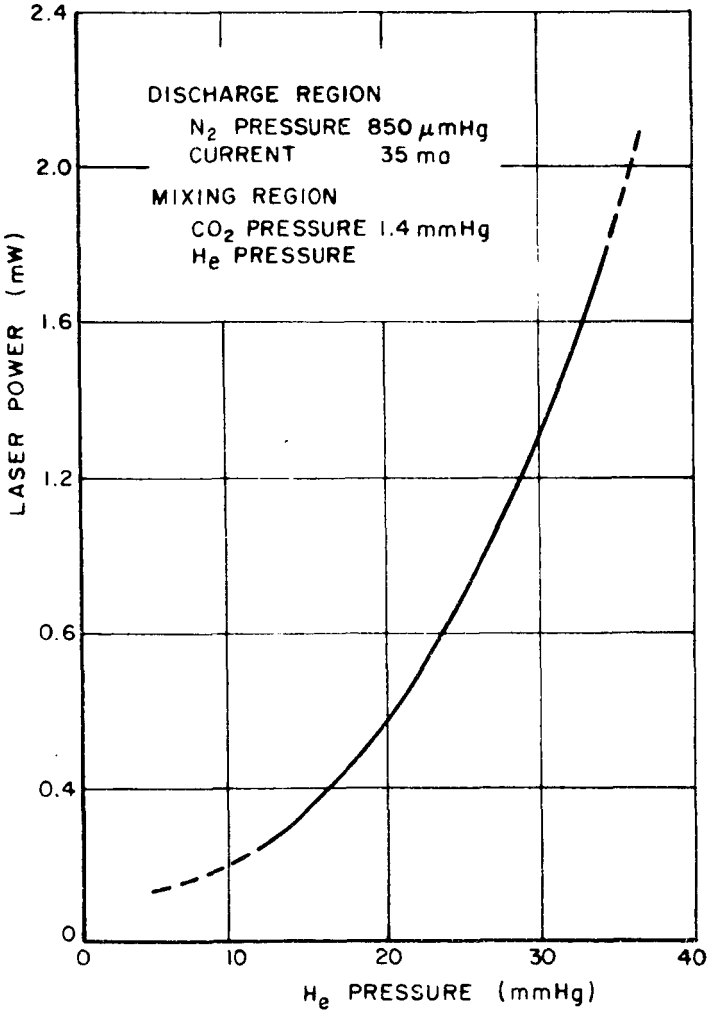

Fig. 17. Laser power for "double-tube" as a function of unexcited He pressure.

was thereby quenched at all He pressures. The writer felt that by adding He in the discharge region, the electron temperature was sufficiently reduced so as to prevent excitation of $N_2(V=1)$.

The enhancement of laser action caused by the addition of He can be explained with the findings of Weber and Deutsch.[16] They showed that upon addition of He to a CO_2 discharge, the relaxation rate of the terminal laser level $CO_2(01^\circ 0)$ is enhanced. This increase in the population inversion increases laser power. The fact that He doesn't have to be mixed with CO_2 in the discharge region to increase laser action can be explained by the results of Schwartz, Slawsky, and Hertzfeld.[15] They showed that the relaxation rate of a pure gas, as compared with a gas mixture that has a reduced mass μ much smaller than the pure gas, is smaller than the relaxation rate for a gas mixture. Thus, the increased laser action of CO_2 by He is partially attributed to the reduced mass μ of the two molecules.

The explanation of Weber and Deutsch also may be used to explain the decrease in CO_2-N_2 laser power with relatively low currents (see Fig. 15). Since the terminal laser level is close to ground level, it is easily populated by electron collisions with CO_2 $(00^\circ 0)$ molecules, and therefore CO_2-N_2 laser action is quenched at relatively low currents; whereas the CO_2-N_2-He laser has an increased relaxation rate which overrides the population buildup caused by electron collisions.

3. CO_2 laser output as a function of discharge tube length

In determining the CO_2-N_2-He laser power as a function of tube length, the tube diameter was at 1.9 cm and the end mirrors were kept at a fixed separation. The gas mixture was set for optimum power and the discharge current set at 50 mA. The total power output obtained is plotted in Fig. 18 for tube lengths of 38 to 160 cm. The results show that power output is approximately a linear function of tube length and that the laser output is approximately 80 mW per cc.

4. CO_2 laser output as a function of discharge tube width and gas flow rate

In determining the CO_2-N_2-He laser power as a function of tube width, the tube length was set at 115 cm. A 1.0 cm iris was placed in the cavity so that only the fundamental mode would oscillate. For each particular tube width the optimum gas pressure was determined. The gas flow rate corresponding to this pressure was then decreased in steps of 1/7 while constant pressure was maintained by regulating the main vacuum valve (see Fig. 12). The results plotted in Figs. 19-23 show how laser power varied with changes in these parameters as discharge current was varied from 0 to 80 mA. There are several results from these graphs that should be noted.

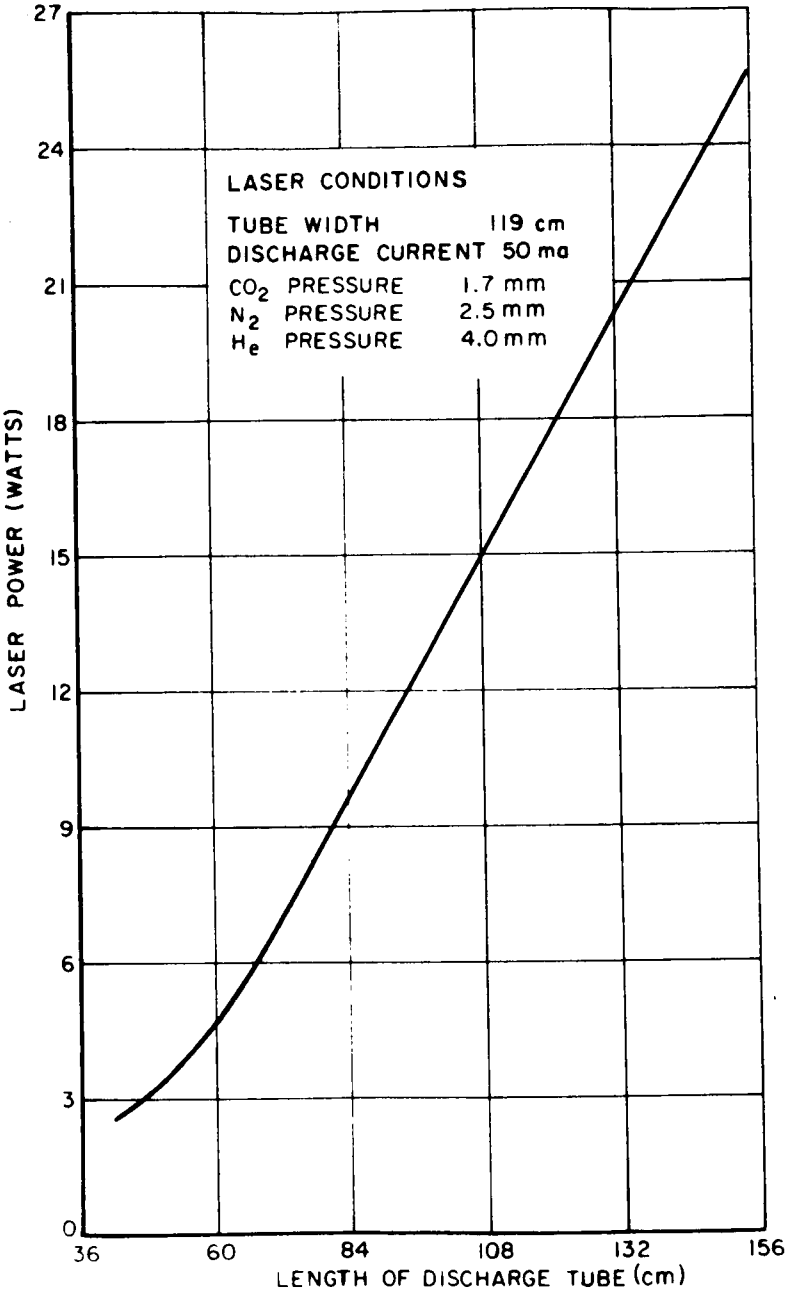

Fig. 18. Laser power output of a CO_2 laser versus discharge tube length.

(a) Laser power was definitely affected by gas flow rate for all tube widths used in this measurement. Laser power steadily increased with increasing flow rate. For the 1.9 cm tube diameter the output laser power as a function of flow rate has been plotted in Fig. 24. Peak output power increased approximately 70% from the value obtained at 2/7 optimum gas flow rate. This percentage increase is even higher if the results are plotted with a fixed current. The writer felt that the effect of gas flow on laser power was mainly because of reduced gas temperature which was caused by high flow rates. Lowering the gas temperature causes less thermal population of the CO_2 lower terminal level. This assumption is further supported by the second result.

(b) Laser power decreases with increasing discharge current at low flow rates. This effect is more pronounced in smaller tube diameters because of higher electron densities for a given discharge current. In Fig. 19, laser power does not drop off even for the lowest flow rate indicated, but in Fig. 23 laser power is zero for a discharge current above 40 mA when the flow rate is at 2/7 of its optimum value. The cause of this effect is based on the same assumption that was stated in the first result.

(c) The third result is the variation of peak power with tube width. Figure 25 is a plot of this result for both a CO_2-N_2-He laser and a CO_2-He laser. For both types of lasers, peak power is

obtained at approximately 1.6 cm tube diameter. Since the general shape of the CO_2-He laser is the same as the CO_2-H_2-He laser, it appears that the effect of N_2 on laser action is not affected by tube width.

5. CO_2 laser output as a function of tube wall temperature

At first the writer felt that wall cooling might increase laser power by 100% or more. He assumed that depopulation of the lower laser level and the lower terminal level of CO_2 would be increased with wall cooling. Figure 26 shows that for the case of a CO_2-N_2-He laser, power output increased only 15% with a 70°C decrease in wall temperature. For the CO_2-He and CO_2-N_2 laser, power increased 45%. Thus, if either N_2 or He gas is omitted, the population inversion rate is decreased and the effect of wall temperature becomes more important on laser action. It appears then that for a 1.9 cm tube diameter, wall cooling is not an important factor in increasing laser power.

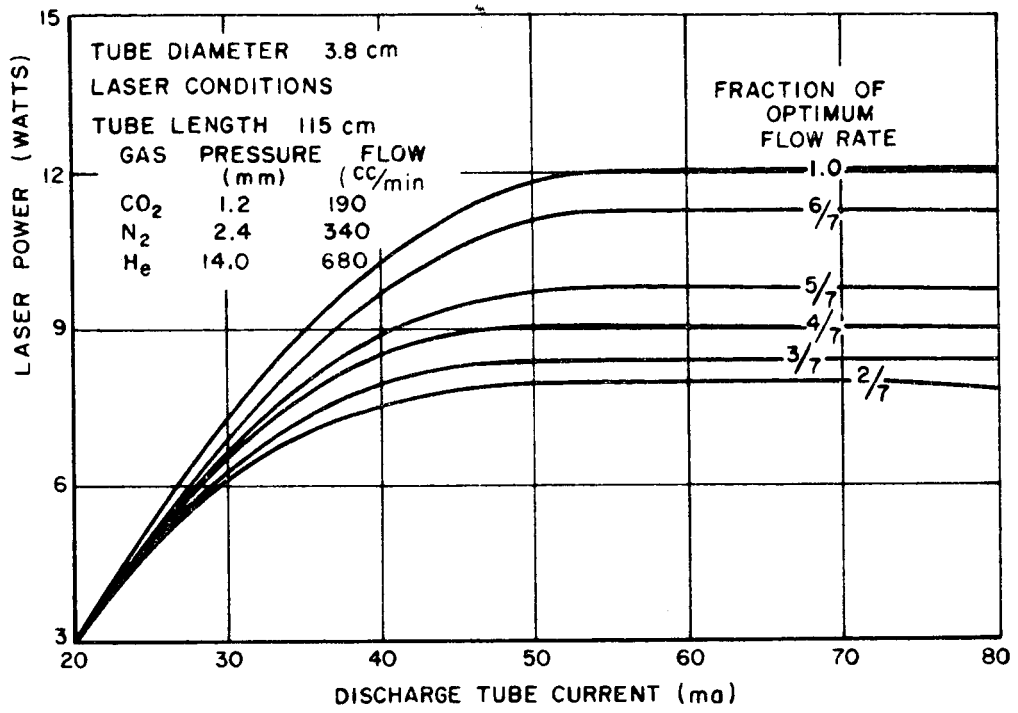

Fig. 19. Laser output as a function of discharge current and gas flow rate.

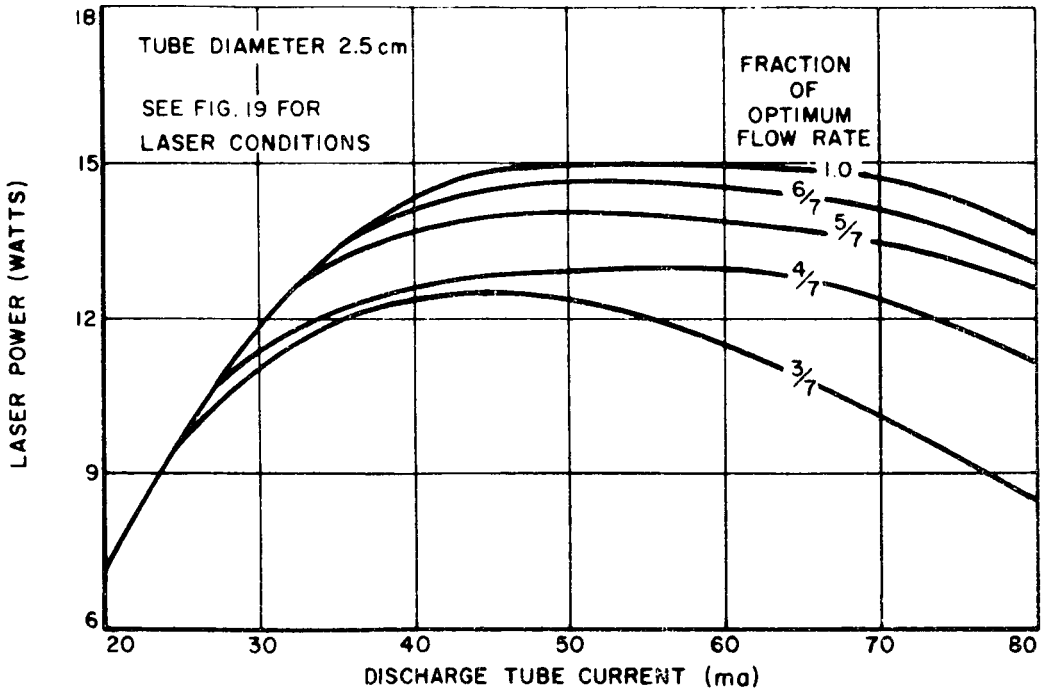

Fig. 20. Laser output as a function of discharge current and gas flow rate.

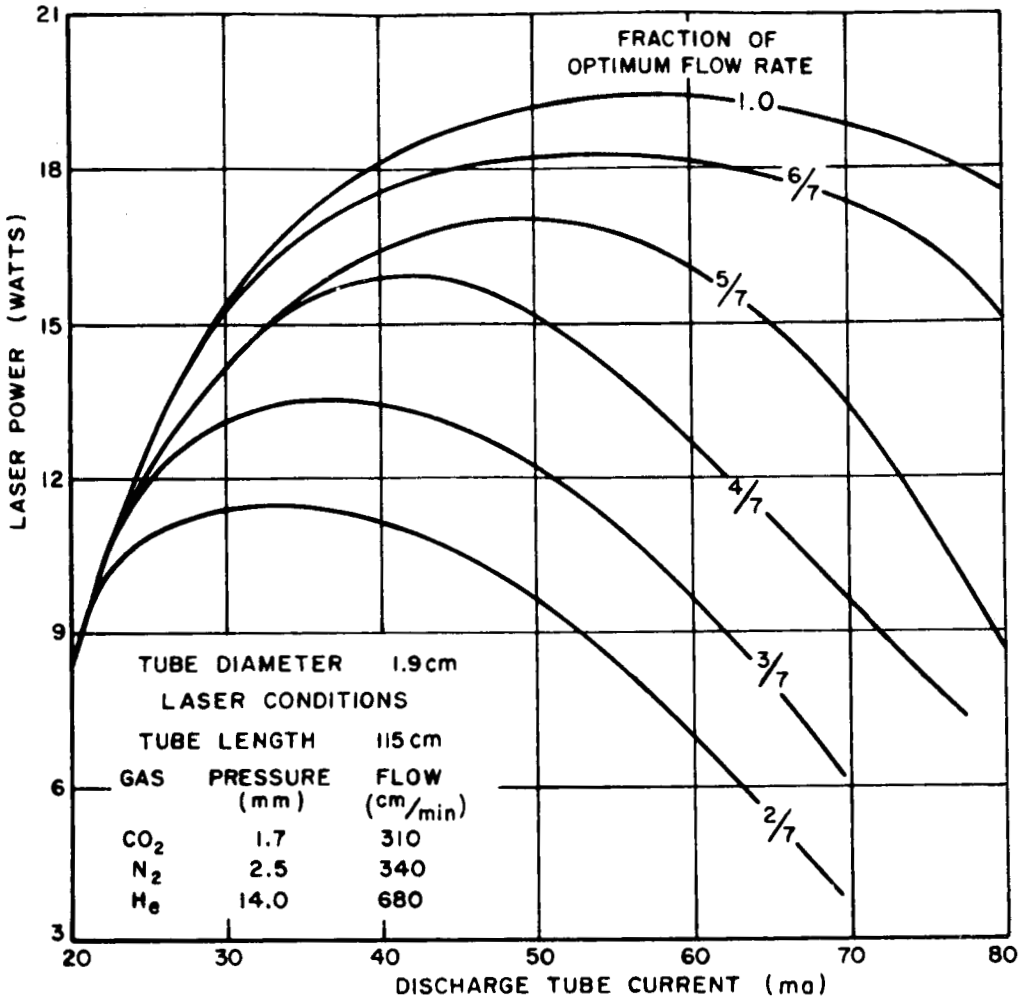

Fig. 26. Laser output as a function of discharge current and gas flow rate.

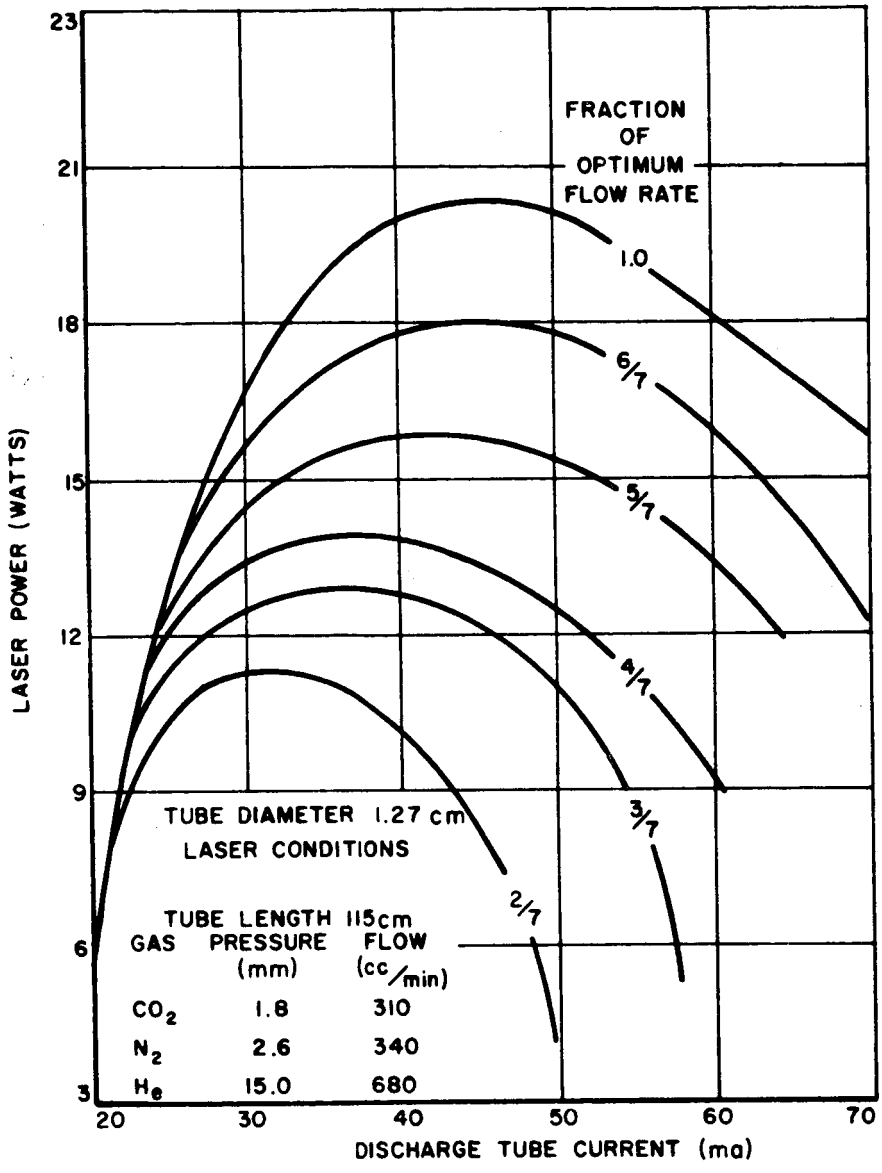

Fig. 22. Laser output as a function of discharge current and gas flow rate.

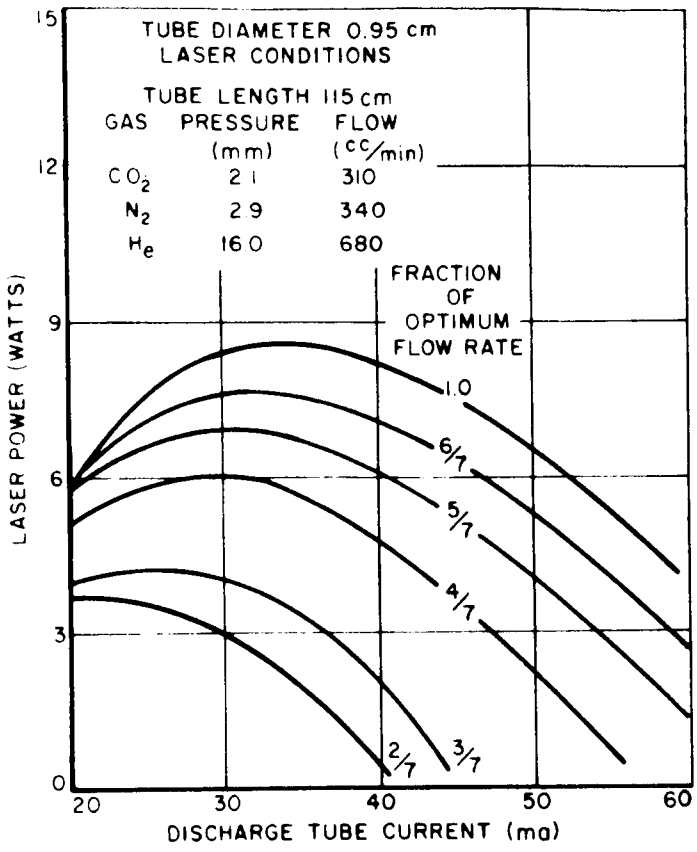

Fig. 23. Laser output as a function of discharge current and gas flow rate.

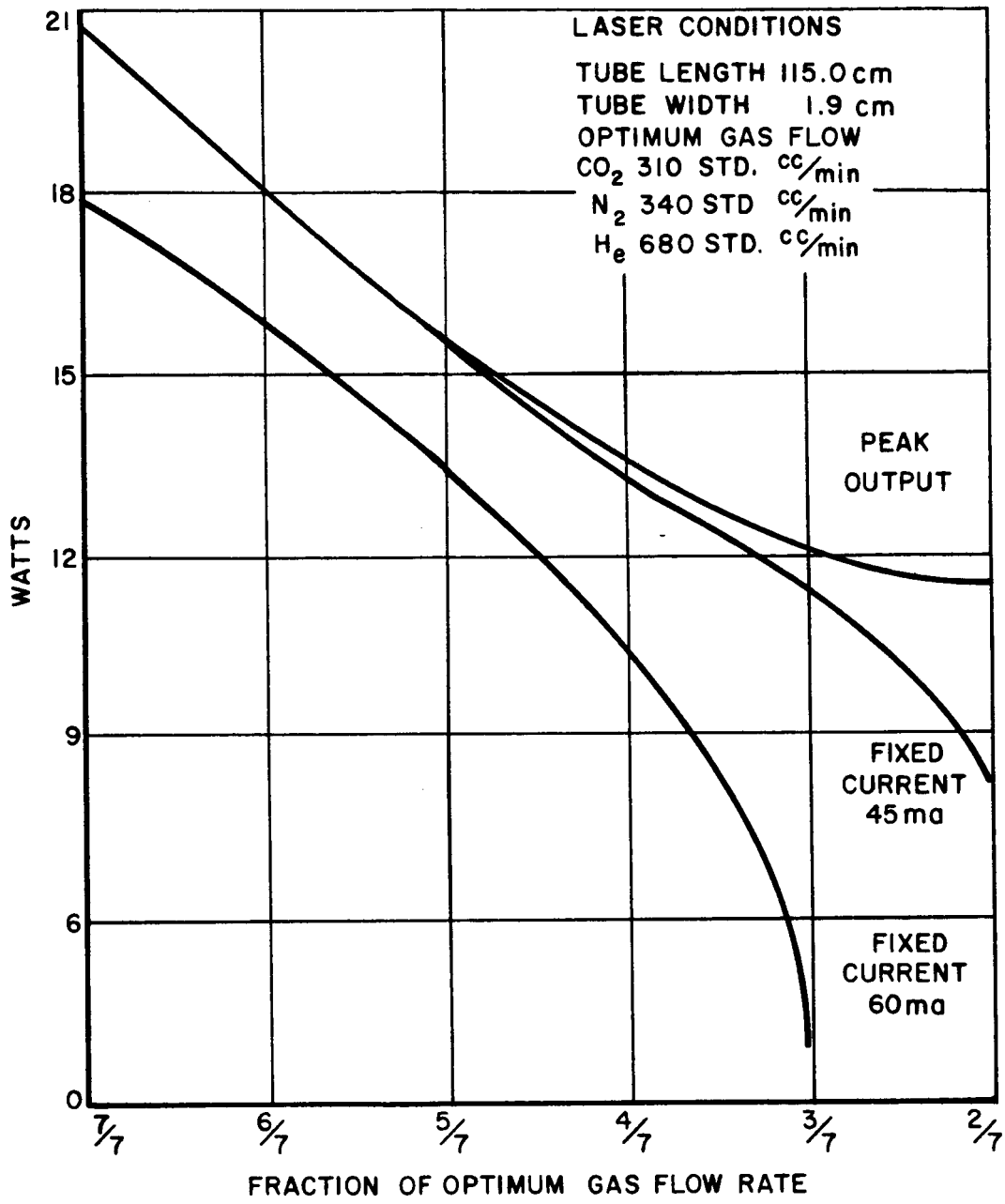

Fig. 24. Laser output as a function of discharge current and gas flow rate.

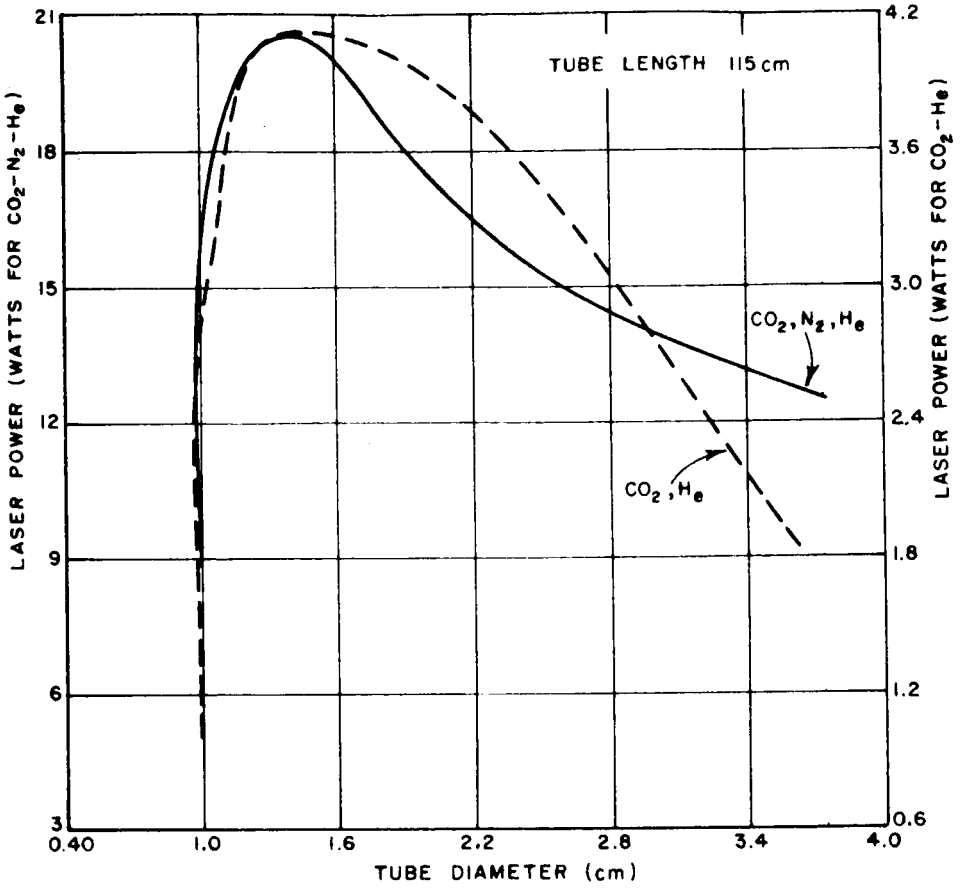

Fig. 25. Optimum laser output as a function of discharge tube diameter.

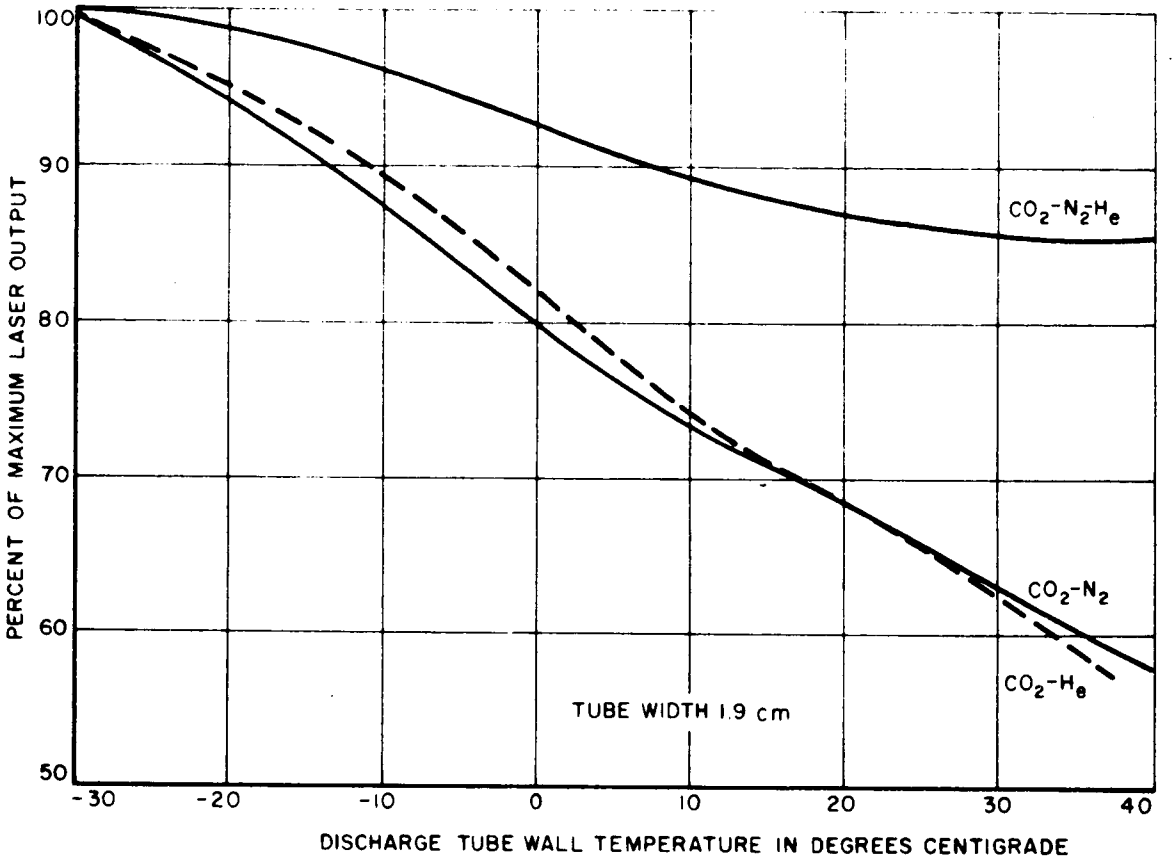

Fig. 26. Laser output as a function of wall temperature and gas mixture.

CHAPTER IV
CONCLUSIONS

The work that has been performed has shown that the effect of certain parameters on CO_2 laser action can be determined. It has been shown that for optimum laser power it is necessary to construct long discharge tubes which have a diameter approximately equal to 1.6 cm. It is necessary to maintain a high gas flow rate and a discharge current of approximately 50 mA. It is necessary also to add He gas to the CO_2-N_2 mixture, but it is not necessary for the He gas to be excited by electron collisions to enhance laser action. Cooling the tube walls of a CO_2 laser increases laser power but only by small percentages. Thus, we do not believe that the additional power received compared to the work necessary for cooling justifies its use.

Direct application of the results found in this work, if optimum laser power is desired at all times, is the ability to design a CO_2 gas laser with these parameters fixed rather than incorporating into the system devices which are necessary to vary these parameters.

Further applications of the "double-tube" experiment may be extended to gas lasers which use a gas that is unstable under discharge; that is, a gas which forms solid deposits on tube walls when under electron bombardment. In using the "double tube," the unstable

gas is placed in the mixing region, out of the discharge, and the gas is excited by molecular collisions from molecules of another gas which were excited by electron collisions in the discharge region.

REFERENCES

1. Patel, C. K. N., "Continuous-Wave Laser Action on Vibrational-Rotational Transitions of CO_2," Phy. Review, Vol. 136, November, 1964.

2. Heine, V., Group Theory in Quantum Mechanics, The MacMillan Company, New York, 1964.

3. Tinkham, M., Group Theory in Quantum Mechanics, McGraw-Hill Book Co., New York, 1964.

4. Smirnov's, V. I., Linear Algebra and Group Theory, McGraw-Hill Book Co., New York, 1961.

5. Townes, C. H., and Schawlow, A. L., Microwave Spectroscopy, McGraw-Hill Book Co., New York, 1955.

6. Herzberg, F. R., Molecular Spectra of Diatomic Molecules, D. Van Nostrand Co., New York, 1959.

7. Herzberg, F. R., Molecular Spectra and Molecular Structure II, Infrared and Raman Spectra of Polyatomic Molecules, D. Van Nostrand and Co., Princeton, New Jersey, 1945.

8. Messiah, A., Quantum Mechanics, John Wiley and Sons, Inc., New York, 1962.

9. Bermbaum, G., Optical Masers, Supplement 2, Academic Press, New York and London, 1964.

10. Patel. C. K. D., "Interpretation of CO_2 Optical Maser Experiments," Phys. Review Letters, vol. 12, No. 21, 1964.

11. Louisell, W., Radiation and Noise in Quantum Electronics, McGraw-Hill Book Co., New York, 1964.

12. Patel, C. K. D., "Selective Excitation Through Vibrational Energy Transfer and Optical Maser Action in N_2-CO_2," Phy. Review, vol. 13, No. 21, 1964.

13. Howe, J. A. and McFarland, R. A., "New Emission System in CO_2," Bell Telephone Lab. Memorandum, October 1965.

14. Bates, D. R., Discussions Faraday Soc., vol 33, No. 7, 1962.

15. Schwartz, R. N., Slawsky, Z. I., and Herzfeld, K. F., "Calculations of Vibrational Relaxation Times in Gases," J. Chemistry Phys., vol. 20, pp. 1591-1599, 1952.

16. Weber, M. J. and Deutsch, T. F., "Pulsed and Steady-State Infrared Emission Studies of CO_2 Laser Systems," Quantum Electronics Conference.

17. Boyd, G. D. and Gordon, J. P., "Generalized Confocal Resonators Theory," Bell System Tech. Journal, vol. 41, pp. 489-508, 1961.

18. Canadian Journal of Physics, vol. 35, 1957.

19. Dennison, D. M., Review of Modern Phy., vol. 12, No. 175, 1940.

20. Moeller, G. and Rigden, J. D., "Recent Developments in CO_2 Lasers," Research Department, Perkin-Elmer Corp., Norwalk, Conn.

21. Moeller, G. and Ridgen, J. D., "High-Power Laser Action in CO_2-He Mixtures," Applied Phy. Letters, vol. 7, No. 10, 1965.